

**Imaging and quantifying the different crystalline
structures of polypropylene with the atomic force
microscope**

By

Abdalah Klash



**Thesis Presented in Partial Fulfilment of the Degree of Master of Science
(Polymer Science)**

at the

University of Stellenbosch

Supervisor: Dr. M. Meincken

Stellenbosch

Co-supervisor: Dr. A. van Reenen

April 2006

Declaration

I the undersigned hereby declare that the work contained in this thesis is my own original work and has not previously in its entirety or in part been submitted at any university for a degree.

Signature:

Date:

Abstract

Isotactic polypropylene (iPP) exists in four different crystalline phases: α -, β -, γ - and the mesomorphic (smectic) form. The α -phase is probably the most predominant form of iPP with a monoclinic unit cell, whereas the unit cell of the γ -phase is orthorhombic. The aim of this study was to examine the ability of AFM to identify the α and γ crystalline forms of polypropylene and polypropylene copolymers that were not especially treated.

Spherulites imaged on propylene-ethylene random copolymer surfaces had diameters ranging from 10-30 μ m and predominantly radial lamellae. The cross-hatching phenomenon of isotactic polypropylene was observed for samples containing both the α - and γ -phase. Two types of γ -phase spherulites were observed, namely a feather-like form for samples with a high content of the γ -phase and a bundle-like form with varying sizes, which is typical for the mixed structure of both α - and γ -forms. In some images of polypropylene-ethylene copolymer sample lozenge-shaped structures could be observed between the γ -spherulites, which might be single polyethylene crystals.

Both the α - and γ -phase of iPP were successfully imaged and identified with AFM without prior treatment of the surface. The degree of crystallinity obtained from AFM images was calculated as a percentage of the surface area exhibiting regular structures. The results compared well to X-ray results.

Opsomming

Isotaktiese polipropileen (iPP) kom in vier verskillende kristallyne vorms voor, naamlik α , β , γ en die mesomorfiëse (smektiese) vorm. Die α fase kom die mees algemeen voor, en het 'n monokliniese eenheidssel, terwyl die γ fase orotorombies is. Die doel van hierdie studie was om die vermoë van die AM om die α en γ kristallyne vorms te kan identifiseer van polimere, wat nie spesifiek behandel om hierdie vorms duidelik sigbaar te maak nie, te ondersoek.

Sferuliete van statistiese kopolimere van etileen en propileen wat ondersoek is, het deursnitte van 10-30 μ m gehad en die voorkoms van radiale lamellae was dominant. Die kruisstruktuur fenomeen wat by isotaktiese polipropileen voorkom is waargeneem vir monsters wat beide die α en γ fases besit. Twee tipes γ fase sferuliete is waargeneem, 'n veeragtige vorm vir monsters met 'n hoë inhoud γ fase, en 'n bundelagtige vorm wat tiperend is van gemengde α en γ vorme. In sommige beelde van propileen-etileen kopolimere is diamant-vormige strukture waargeneem tussen die γ sferuliete, wat moontlik polietileen enkelkristalle kon wees.

Beide die α en γ fase van iPP is suksesvol geïdentifiseer deur AM sonder voorafbehandeling van die oppervlak van die polimeer. Die graad van kristallasie vanaf AM beelde verkry is bereken as persentasie van die oppervlak waar geordende strukture sigbaar was. Die resultate vergelyk goed met X-straal diffraksie metings.

Acknowledgments

First and foremost, I would like to express my most sincere thanks to my advisor and supervisor, Dr. M. Meincken, for her continuous guidance and support throughout this work. I am also sincerely grateful to Dr. A. Van Reenen, my co-supervisor, for his invaluable advice, guidance and assistance, which led to the completion of this project. It was an honour to know and to work with them.

I would also like to thank G. Harding and M. Lutz for their help and support and also for generously allowing the use of some of their samples.

Furthermore, I am thankful to all the members of Chemistry and Polymer Science Department for their cooperation and time.

I also acknowledge the financial support received from the International Centre for Macromolecular Chemistry and Technology in Libya.

Finally, I would like to dedicate this thesis to my family for their continuous love and encouragement and to my friends for their help and support.

A large part of this thesis was presented as a poster at the
IUPAC New Directions in Chemistry Workshop on Advanced
Materials (WAMIII) focusing on Nanostructured Advanced
Materials.

This conference took place 5-8 September 2005, at the
University of Stellenbosch, South Africa.

IDENTIFYING DIFFERENT CRYSTALLISATION FORMS OF ISOTACTIC POLYPROPYLENE WITH ATOMIC FORCE MICROSCOPY



A. Klash, A. van Reenen, M. Meincken

Department for Chemistry and Polymer Science, Polymer Science, University of Stellenbosch, Private Bag X1, Matieland 7602, South Africa, email: mmein@sun.ac.za

Introduction

Isotactic-Polypropylene exists in four different crystalline modifications: α -, β -, γ - and the mesomorphic (smectic) form. They have in common the three-folded chain helix configuration with a repeat distance of 6.5Å, which the chain assumes in order to relieve the steric hindrance, which is caused as a result of the presence of the methyl-groups along the chain backbone. The α -modification is probably the most predominant form of iPP with a monoclinic unit cell with the following cell parameters: a = 6.65Å, b = 20.96Å, and c = 6.5Å. The unit cell of the γ -modification is orthorhombic with the parameters: a = 8.54 Å, b = 9.93Å, and c = 42.41 Å [1, 2].

Atomic force microscopy (AFM) has proved to be a very powerful tool to resolve the structure and molecular packing of isotactic polypropylene [2-4]. All these studies, however, were performed on especially prepared iPP surfaces (etched or epitaxially grown from benzoic acid substrates) for AFM investigation, in order to obtain the high resolution necessary to identify the different crystallisation forms.

In this study AFM was used to differentiate and identify different crystallisation forms of isotactic polypropylene without any special prior preparation.

Materials & Methods

Sample preparation:

1) Isotactic polypropylene
Isotactic polypropylene pellets were hot-pressed at 190°C into a film. This film of α -iPP was then crystallized in an isothermal process at 130°C for 24h in vacuum. Subsequently it was cooled down to room temperature at cooling rate of 20°C/h.

2) Propylene-ethylene co-polymer
Samples of α - and γ -phase PPE-copolymer (1.8-3.25% ethylene) were hot-pressed at 230°C into 100µm thick films, then melted at 180°C in vacuum, and subsequently slowly cooled to room temperature at a rate of 2°C/h.

Instrument:

AFM measurements were performed with a Multimode AFM with a Nanoscope III controller from Veeco under ambient conditions. The AFM was operated in contact mode.

AFM calibration

The piezo scanner of the AFM was calibrated on a freshly cleaved mica surface was used. Images were acquired with the A-scanner and a V-shaped contact cantilever. The distances measured after the calibration showed an inaccuracy of less than 2%.

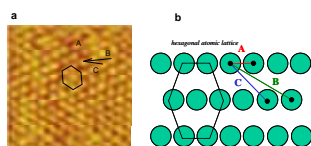


Figure 1: a) Fourier-filtered AFM image of mica with a size of 6x6nm² indicating the measured distances A=0.528 nm, B=1.379 nm, C=0.909nm. b) The schematic drawing shows the expected distances of A=0.519 nm, B=1.37nm, C=0.900nm

Results

1) α -modification

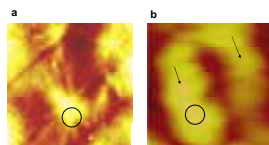


Figure 2: a) Topography image of α -iPP, scan size 50x50 µm² and b) 220x220 nm²

Figure 2a shows typical α -spherulites in iPP with a radius ranging from 10 to 30 µm. Lamellae can be observed in radial direction. Figure 2b shows the lamellar structure with an average thickness of 65 nm. The arrows indicate the radial direction of the lamellae. The circles indicate the areas, where images with higher resolution were acquired.

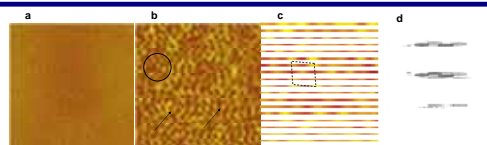


Figure 3: a) Unfiltered AFM image of i-PP, 11x11nm². b) Fourier-filtered version of the same image. Figure 4c shows a section of (b) with a size of 3x3nm². 4d shows the schematic illustration of the ac plane of an α -phase crystal structure (Five pattern)

Figure 3a shows an un-filtered AFM image which was acquired on the lamellar structure in figure 2b. Figure 3b, shows the Fourier transformed image of (3a), in which the methyl groups are revealed, which are arranged in a lozenge-shaped pattern. The chain direction is almost normal to the lamellar surface. Figure 3c shows a higher resolution image with a scan size of 3x3nm². The methyl groups arranged on the ac plane show a distinctive five pattern, as it is common for the α -modification of the crystal structure. Figure 3d shows an illustration of the ac plane of the α -modification as suggested by Lotz [2]

2) γ -modification

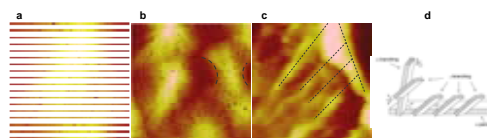


Figure 4: a) AFM images of a γ -spherulite with a scan size of 60x60 µm², b) 120x120 µm², and c) 1.3x1.3µm². d) Schematic model of α - α -i PP and γ - α -i PP branching [3].

Figure 4a shows the spherulite morphologies of the γ -modification consisting of lamellae in a feather-like structure. The form of the lamellae can be explained either by an epitaxial crystallization of γ -lamellae with an 40° angle to the radial α -lamellae, or by branching of the γ -lamellae at an angle of 140° on the surface of another γ -lamella[3]. Figure 4b visualizes the bow-tie shaped spherulites, with varying sizes, which is typical for the mixed structure of both α - and γ -forms [4]. Figure 4c shows the epitaxial ongrowth of γ -lamellae on a α -lamella at an angle of approximately 45°.

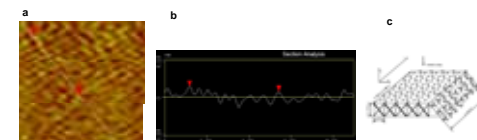


Figure 5: a) High resolution image with a scan size of 7x7 nm². b) height profile along the line drawn in (a). c) schematic drawing of the 110 plane of the γ -phase with dimensions and the arrangement of helices [4].

Figure 5a shows the methyl groups as bright spots. Although they appear disordered, one can distinguish rows, which are oriented normal to the line drawn in the figure. Figure 5b shows the height profile along the line in (5a) across rows of methyl groups. The average distance between 12 rows was about 42.52Å, compared to 42.41Å expected theoretically [1]. The repeat unit on the 110 surface in the γ -modification is 12 rows. Figure 5c shows a schematic representation of the crystal lattice with dimensions and the arrangement of helices in the (110) plane of the γ -phase.

Conclusions

The results show that AFM is able to study the polymer morphology at a molecular level. Both α - and γ -iPP have been successfully imaged and identified without special preparation or prior treatment surfaces.

References

- [1] S. Bruckner, S.V. Meille, V. Petraccone, B. Pirozzi, *Prog. Polym. Sci.* 1991, 16(2-3), 361-404.
- [2] B. Lotz, J.C. Wittmann, A.J. Loving, *Polymer* 1996, 37 (22), 4979-4992.
- [3] I.L. Hoser, R.G. Alamo, J.S. Lin, *Polymer* 45 3441-3455, 2004
- [4] R. Thomann, C. Wang, J. Kressler, R. Mülhaupt, *Macromolecules*, 29, 8425, 1996

Acknowledgements

The authors would like to thank the International Centre for Macromolecules Chemistry and Technology in Libya for financial support.

TABLE OF CONTENTS

1	INTRODUCTION	1
1.1	OBJECTIVES.....	2
1.2	LAYOUT OF THE THESIS.....	2
1.3	REFERENCES.....	3
2	THEORETICAL BACKGROUND	5
2.1	POLYPROPYLENE.....	5
2.1.1	<i>POLYPROPYLENE POLYMERIZATION.....</i>	5
2.1.1.1	Ziegler-Natta catalysts	5
2.1.1.2	Metallocene catalysts	5
2.1.2	<i>POLYPROPYLENE CONFIGURATIONS</i>	6
2.1.3	<i>POLYPROPYLENE CONFORMATIONS AND CRYSTAL STRUCTURES</i>	7
2.1.4	<i>CRYSTALLINITY AND POLYMER STRUCTURE</i>	8
2.2	THE CRYSTALLINE STRUCTURE OF ISOTACTIC POLYPROPYLENE (iPP).....	9
2.2.1	<i>THE α-PHASE OF ISOTACTIC POLYPROPYLENE</i>	9
2.2.1.1	The unit cell of the α -phase	9
2.2.1.2	The lamellar structure of the α -phase	11
2.2.1.3	The spherulite structure of the α -phase	12
2.2.2	<i>THE β-PHASE OF ISOTACTIC POLYPROPYLENE</i>	13
2.2.2.1	The unit cell of the β -phase	13
2.2.2.2	The lamellar structure of the β -phase	14
2.2.2.3	The spherulite structure of the β -phase.....	15
2.2.3	<i>THE γ-PHASE OF ISOTACTIC POLYPROPYLENE.....</i>	15
2.2.3.1	The unit cell of the γ -phase	16
2.2.3.2	The lamellar structure of the γ -phase.....	18
2.2.3.3	The spherulite structure of the γ -phase	19
2.2.4	<i>MESOMORPHIC (SMECTIC) PHASE OF ISOTACTIC POLYPROPYLENE</i>	21
2.3	POLYPROPYLENE COPOLYMERS	22

2.3.1	<i>RANDOM COPOLYMERS</i>	22
2.3.2	<i>IMPACT (BLOCK) COPOLYMERS</i>	22
2.4	REFERENCES	24
3 INSTRUMENTATION		29
3.1	ATOMIC FORCE MICROSCOPY (AFM)	29
3.1.1	<i>AFM OPERATION</i>	29
3.1.2	<i>AFM OPERATION MODES</i>	31
3.1.2.1	Contact mode	31
3.1.2.2	Non-contact mode	31
3.1.2.3	Tapping mode:	32
3.1.3	<i>ATOMIC RESOLUTION AND NOISE ARTIFACTS</i>	32
3.1.3.1	Probe geometry	32
3.1.3.2	Thermal noise.....	33
3.1.3.3	Mechanical noise	33
3.1.3.4	Electronic noise.....	33
3.2	WIDE ANGLE X-RAY DIFFRACTION (WAXD)	34
3.2.1	<i>BRAGG'S LAW</i>	34
3.2.2	<i>CRYSTAL LATTICE AND INDICES</i>	34
3.2.3	<i>DETERMINATION OF THE DEGREE OF CRYSTALLINITY</i>	36
3.2.4	<i>DETERMINATION OF THE γ-PHASE CONTENT</i>	37
3.3	REFERENCE	38
4 EXPERIMENTAL		41
4.1	MATERIALS AND SAMPLE PREPARATION	41
4.1.1	<i>ISOTACTIC POLYPROPYLENE</i>	41
4.1.2	<i>PROPYLENE-ETHYLENE RANDOM COPOLYMERS</i>	41
4.1.3	<i>PROPYLENE-ETHYLENE BLOCK COPOLYMERS (IMPACT POLYPROPYLENE)</i>	42
4.1.4	<i>PROPYLENE-PENTENE RANDOM COPOLYMERS</i>	43
4.2	PERMANGANIC ETCHING OF THE SAMPLES	43
4.3	INSTRUMENTATION	44
4.3.1	<i>WIDE ANGLE X-RAY DIFFRACTION (WAXD)</i>	44

4.3.2	<i>ATOMIC FORCE MICROSCOPE</i>	44
4.3.2.1	AFM calibration.....	44
4.3.2.2	Sample imaging	45
4.4	DIFFICULTIES	48
4.5	REFERENCE	50
5	RESULTS AND DISCUSSION	51
5.1	WIDE-ANGLE X-RAY DIFFRACTION	51
5.1.1	<i>ISOTACTIC POLYPROPYLENE</i>	52
5.1.2	<i>PROPYLENE-ETHYLENE RANDOM COPOLYMERS</i>	53
5.1.3	<i>PROPYLENE-ETHYLENE BLOCK COPOLYMERS</i>	55
5.1.4	<i>PROPYLENE-PENTENE RANDOM COPOLYMERS</i>	56
5.2	ATOMIC FORCE MICROSCOPY	57
5.2.1	<i>ISOTACTIC POLYPROPYLENE</i>	57
5.2.2	<i>PROPYLENE-ETHYLENE RANDOM COPOLYMERS</i>	58
5.2.2.1	The α -phase	58
5.2.2.2	The γ -phase	62
5.2.3	<i>PROPYLENE-ETHYLENE BLOCK COPOLYMERS</i>	67
5.2.4	<i>PROPYLENE-PENTENE RANDOM COPOLYMERS</i>	70
5.3	ATTEMPTED QUANTIFICATION THE DEGREE OF CRYSTALLINITY	71
5.4	REFERENCES	77
6	CONCLUSIONS AND SCOPE OF FUTURE WORK	79
6.1	CONCLUSIONS	79
6.2	SUGGESTED FUTURE WORK	80
6.3	REFERENCES	82

List of Abbreviations

AFM	Atomic force microscopy
Cp	Cyclopentadienyl
dw	Down
EP	Ethylene-Propylene
G	Gauche
iPP	Isotactic-polypropylene
I_a	Amorphous halo intensity
I_c	Crystalline peaks intensity
I_{tot}	Total scattering intensity
KJ	Kilo Joule
L	Left-handed
MAO	Methylalumoxane
Mt	Transition metal
N	Newton
R	Right-handed
SAXD	Small angle X-ray diffraction
SEM	Scanning electron microscopy
Si	Silicon
Si_3N_4	Silicon nitride
STM	Scanning tunnelling microscope
t	Trans
TEM	Transmission electron microscopy
T_m^o	Melting point

up

WAXD

ΔH_f°

ω_m

Up

Wide angle X-ray diffraction

Heat of fusion

Mass crystallinity

List of Figures

Figure 2. 1: Schematic illustration of the stereochemical configurations of polypropylene: a) isotactic, b) syndiotactic, c) atactic.....	6
Figure 2. 2: Illustration of the helical structure of isotactic polypropylene: a) right-handed, b) left-handed helices. The continuous line shows the up direction and the dashed line the down direction of the methyl groups.	8
Figure 2. 3: Illustration of the two crystallization types of α -iPP, a) the $\alpha 1(C2/c)$ and b) the $\alpha 2 (P2_1/c)$	10
Figure 2. 4: Schematic illustration of the two possible surface structures of the a-c (010) plane of α -iPP, a) four-face pattern, b) five-face pattern.	11
Figure 2. 5: Schematic illustration of α - α iPP lamellae branching (cross-hatched structure)	12
Figure 2. 6: Optical micrograph of α -iPP spherulites, a) type I crystallized at 130°C, b) type II crystallized at 140°C.	13
Figure 2. 7: Schematic representation of the arrangement of iPP-helices in the β -phase. The lines indicate the a- and b-axes; the c-axis is perpendicular to the plane of view	14
Figure 2. 8: SEM micrograph of an etched banded β -spherulite type β IV crystallized at 130°C.	15
Figure 2. 9: Schematic representation of the arrangement of iPP-helices in the γ -phase.	17
Figure 2. 10: Schematic illustration of the crystal lattice with dimensions and the arrangement of helices in the (110) plane of the γ -phase.	18
Figure 2. 11: Schematic illustration of the γ - α branching.	19
Figure 2. 12: Reflection optical micrograph of lamellae in iPP crystallized at 200 MPa and an isothermal crystallization temperature of 203°C. Lamellae are arranged in the form of feathers. The sample was etched with permanganate potassium for 30 minutes.....	20
Figure 2. 13: a) Epitaxial growth of γ -lamellae on α -lamellae, b) epitaxial growth of γ lamellae on γ -lamellae.	20
Figure 2. 14: Polarized light micrographs taken during isothermal crystallization of	

metallocene iPP at 120°C after crystallization times: a) 1:50 h, b) 4:30 h, c) 23 h and d) 43 h	21
Figure 3. 1: Schematic illustration of the atomic force microscope, showing the: probe, cantilever, photodetector, scanner, computer control, and sample.....	29
Figure 3. 2: Schematic illustration of the interatomic forces acting between tip/sample atoms for contact, non-contact and tapping mode imaging.	30
Figure 3. 3: An illustration of the conditions of diffraction in Bragg's law	34
Figure 3. 4: A schematic illustration of the unit cell and the (110) plane	35
Figure 3. 5: A typical X-ray diffraction pattern of pure, a) α -, b) β - and c) γ -phase of iPP.....	36
Figure 3. 6: Scattering Curve for isotactic polypropylene showing the crystalline peaks and the amorphous background scattering	37
Figure 4. 1: a) Fourier-filtered AFM image of mica with a size of 6x6 nm ² indicating the measured distances A=0.528 nm, B=1.379 nm, C=0.909 nm. b) The schematic drawing shows the expected distances of mica: A=0.519 nm, B=1.37nm, C=0.900nm.	45
Figure 4. 2: a) AFM image of mica before filtering and b) AFM image of mica after filtering, c) Fourier transformed image of mica before filtering, d) Fourier transformed image after filtering.	47
Figure 4. 3: Schematic illustration of the building blocks of iPP crystals.....	49
Figure 5. 1: WAXD pattern of iPP melt crystallized at 130°C.....	52
Figure 5. 2: WAXD pattern of PPE samples melt-crystallized at a slow cooling rate of 2°C/ h.....	53
Figure 5. 3: WAXD pattern of PEB samples melt-crystallized at a slow cooling rate of 2°C/ h.....	55
Figure 5. 4: 3x3 nm ² AFM height images of iPP a) regular structure α -phase, b) amorphous region of the same sample.....	57
Figure 5. 5: 50x50 μ m ² AFM height image of PPE5 with 87.77% of α -phase.	58
Figure 5. 6: 220x220 nm ² AFM image, magnified from figure 5.5.....	59
Figure 5. 7: a) Unfiltered AFM image of PPE5, scan size 11x11nm ² , b) Fourier-	

filtered version of a), c) a section of b) of $3 \times 3 \text{ nm}^2$, d) model produced with X-seed to illustrate the ac plane of a α -phase crystal structure (Five pattern).....	60
Figure 5. 8: AFM micrograph of cross-hatching of PPE2 sample.....	61
Figure 5. 9: AFM images of PPE1 with 73.92% γ -phase with a scan size of a) $100 \times 100 \mu\text{m}^2$, b) $60 \times 60 \mu\text{m}^2$	62
Figure 5. 10: Scheme of the growth mechanism of the feather-like structure of γ lamellae. a) Epitaxial growth of γ -lamellae on α -lamellae. b) Epitaxial growth of γ -lamellae on γ -lamellae.	63
Figure 5. 11: AFM image of γ -phase spherulites with a scan size of $120 \times 120 \mu\text{m}^2$	63
Figure 5. 12: a) AFM image of PPE1 with a scan size of $70 \times 70 \mu\text{m}^2$ and b) acquired from (a) as indicated with a box, scan size of $4.5 \times 4.5 \mu\text{m}^2$	64
Figure 5. 13: a) AFM image of $1.3 \times 1.3 \mu\text{m}^2$ acquired in Figure 12, b) schematic model of α -iPP and γ -iPP branching from an α -‘parent’ lamella. The crystallographic axes are indicated.	65
Figure 5. 14: a) High resolution image with a scan size of $7.1 \times 7.1 \text{ nm}^2$. The methyl groups are arranged in rows. b) the cross section along the line in a) showing the height profile of the methyl group rows, c) schematic drawing of the 110 plane of the γ -phase with dimensions and the arrangement of helices.	66
Figure 5. 15: AFM image of a) PEB1, b) PEB2 and c) PEB3 with scan size $3 \times 3 \mu\text{m}^2$..	67
Figure 5. 16: High resolution AFM image of PEB1 a) $6 \times 6 \text{ nm}^2$, b) $3 \times 3 \text{ nm}^2$ and c) model produced with X-seed to illustrate the ac plane of a α -phase crystal structure (Four pattern)	69
Figure 5. 17: AFM image of a) PPe1, PPe2, PPe3 and PPe4 with scan size of $12.5 \times 12.5 \mu\text{m}^2$	70
Figure 5. 18: High resolution AFM image with a scan range of $6 \times 6 \text{ nm}^2$, b) magnified image with a scan range of $2 \times 2 \text{ nm}^2$	71

List of Tables

Table 4. 1: Characteristics of propylene-ethylene co-polymer samples.....	42
Table 4. 2: Characteristics of propylene-ethylene block copolymers.....	42
Table 4. 3: Characteristics of propylene-pentene random copolymers.....	43
Table 5. 1: Isotactic polypropylene with its degree of crystallinity and the percentage of different crystal phases.	53
Table 5. 2: propylene-ethylene co-polymer samples with their degree of crystallinity and the percentage of different crystal phases.	54
Table 5. 3: Propylene-ethylene block copolymer samples with their degree of crystallinity and the percentage of different crystal phases.	56
Table 5. 4: Propylene-pentene random copolymer samples with their degree of crystallinity and the percentage of different crystal phases.	56
Table 5. 5: Estimation of the average degree of crystallinity for iPP.....	72
Table 5. 6: Estimation of the average degree of crystallinity for PPE5.....	73
Table 5. 7: Estimation of the average degree of crystallinity for PPE1.....	74
Table 5. 8: Estimation of the average degree of crystallinity for PEB3 of the surface showing the four pattern (a).....	75
Table 5. 9: Estimation of the average degree of crystallinity for PBE3 of the surface showing of five pattern (b).....	76

1 Introduction

Isotactic-polypropylene (iPP) exists in four different crystalline modifications: α -, β -, γ - and the mesomorphic (smectic) form. They have in common a three-folded chain helix configuration with a repeat distance of 6.5\AA , which the chain assumes in order to relieve the steric hindrance, which is caused by the methyl-groups along the chain backbone. The α -modification is the most predominant form of iPP with a monoclinic unit cell with the following cell parameters: $a = 6.65\text{\AA}$, $b = 20.96\text{\AA}$ and $c = 6.5\text{\AA}$. The unit cell of the γ -modification is orthorhombic with the parameters $a = 8.54\text{\AA}$, $b = 9.93\text{\AA}$ and $c = 42.41\text{\AA}$ [1-5].

Atomic force microscopy (AFM) has proved to be a very powerful tool to study the topology and physical properties of polymer surfaces [6-10]. Compared to techniques traditionally used to investigate crystalline structures, such as wide angle X-ray diffraction (WAXD) [11], small angle X-ray diffraction (SAXD) and Raman spectroscopy, the AFM has the advantage of direct visual presentation of the morphology on a molecular scale. Also, in comparison with scanning electron microscopy (SEM) and transmission electron microscopy (TEM), AFM does not require surface coating, or any other special preparation, which allows imaging of the real sample surface.

AFM can be used to determine the structure and molecular packing of isotactic polypropylene. Stocker et al. [12, 13] imaged the contact plane evolving when α - or γ -iPP are crystallized on benzoic or nicotinic acid substrates. In their experiments they crystallized iPP epitaxially on the substrate, which was subsequently dissolved with ethanol. The methyl groups of the iPP chains on the contact surface were then visualized with AFM. Thomann et al. [14] reported that AFM analysis on a molecular scale of thin iPP films prepared from solution revealed the methyl groups of the a-c (010) plane of the γ -phase of iPP.

All these studies, however, were performed on specially prepared iPP surfaces (etched or epitaxially grown from benzoic acid substrates), in order to obtain the high resolution necessary to identify the different crystalline forms.

1.1 Objectives

The aim of this study was to examine the ability of AFM to analyze and identify the α and γ crystalline forms of isotactic polypropylene, polypropylene-ethylene random copolymers, polypropylene-ethylene block copolymers (impact polypropylene) and polypropylene-1-pentene copolymers without any further preparation of the polymer films after crystallization from the melt. An attempt would be also made to quantify the amount of the α and γ phase. The degree of crystallinity and the α and γ crystalline content would be determined by WAXD to compare with the AFM results.

1.2 Layout of the thesis

The second chapter of the thesis gives an overview over the polypropylene chain conformations and configurations. It describes in detail the different polymorphisms of isotactic polypropylene from crystal structures to supermolecular structures (spherulites). The third chapter describes the principle and the operation modes of the atomic force microscope and gives a short overview of the principle of wide angle X-ray diffraction and how the degree of crystallinity and the different phase contents were calculated. The fourth chapter describes the sample preparation and the AFM and WAXD set-up. The fifth chapter presents and compares the results obtained by WAXD and AFM. These results are discussed and explained based on the theoretical background provided in Chapters 2 and 3. A correlation between these results is made.

1.3 References

1. S. Brückner, S. V. Meille, V. Petraccone, B. Pirozzi. *Polymorphism of isotactic polypropylene*. Progress in Polymer Science. 1991, **16**, 361-404.
2. D. R. Norton, A. Keller. *The spherulitic and lamellar morphology of melt-crystallized isotactic polypropylene*. Polymer. 1985, **26**, 704-716.
3. F. J. Padden, J. D. Keith. *Spherulitic crystallization in polypropylene*. Journal of Applied Physics. 1959, **30**, 1479-1484.
4. B. Lotz, C. Wittmann, A. J. Lovinger. *Structure and morphology of poly(propylenes): a molecular analysis*. Polymer. 1996, **22**, 4979-4992.
5. G. Natta, P. Corradini. *Structure and properties of isotactic polypropylene*. Nuovo Cimento. 1960, **15**, 40-51.
6. F. J. Giessibl. *Advances in atomic force microscopy*. Reviews of Modern Physics. 2003, **75**, 949-984.
7. M. R. Jarvis, R. Pérez, M. C. Payne. *Can atomic force microscopy achieve atomic resolution in contact mode?* Physical Review Letters. 2001, **86**, 1287-1291.
8. B. D. Ratner, V. V. Tsukruk. eds. *Scanning probe microscopy of polymer*. 1st ed. Orlando: American Chemical Society. 1996, 53-93.
9. S. N. Magonov. *Atomic force microscopy in analysis of polymers*, in *Encyclopedia of Analytical Chemistry*, R.A. Meyers, Editor. Wiley. 2000, 7433-7490.
10. C. Mathieu, A. Thierry, J. C. Wittmann, B. Lotz. *“Multiple” nucleation of the (010) contact face of isotactic polypropylene, α -phase*. Polymer. 2000, **41**, 7241-7253.
11. C. Y. Li, B. Wang, S. Z. Cheng. *X-ray Scattering in analysis of polymers*, in *Encyclopaedia of Analytical Chemistry*, R.A. Meyers, Editor. Wiley. 2000, 8105-8118.
12. W. Stocker, S. N. Magonov, H. J. Cantow, J. C. Wittmann, B. Lotz. *Contact Faces of epitaxially crystallized α - and γ -Phase isotactic polypropylene observed by atomic force microscopy*. Macromolecules. 1993, **26**, 5915-5923.
13. W. Stocker, M. Schumacher, S. Graff, A. Thierry, J. C. Wittmann, B. Lotz. *Epitaxial crystallization and AFM investigation of a frustrated polymer*

structure: isotactic poly(propylene), β -Phase. Macromolecules. 1998, **31**, 807-814.

14. R. Thomann, C. Wang, J. Kressler, R. Muelhaupt. *On the γ -Phase of isotactic polypropylene.* Macromolecules. 1996, **29**, 8425-8434.

2 Theoretical Background

2.1 Polypropylene

2.1.1 Polypropylene polymerization

There are two main types of catalysts, with which propylene monomers alone, or together with a co-monomer, can be polymerized to form polypropylene. These are Ziegler-Natta and Metallocene catalysts.

2.1.1.1 Ziegler-Natta catalysts

Polypropylene with a high molecular weight became available and commercially interesting after the discovery of a new catalyst by Ziegler and Natta in 1953 [1, 2]. Before that time propylene was polymerized via a reaction with concentrated sulfuric acid [3]. The product obtained had a low molecular weight (oligomers) and was a viscous oil with limited industrial applications [4]. Ziegler-Natta catalysts made the production of high molecular weight polypropylene possible, and enabled the control of the stereospecificity of the propene addition during polymerization (i.e. isotactic, syndiotactic and atactic polypropylene). The catalysts are based on transition metal-chloride and alkyl aluminium complexes, TiCl_4 or TiCl_3 , as catalyst and $\text{Al}(\text{Et}_3)$ or $\text{Al}(\text{Et}_2)\text{Cl}$ as co-catalysts [4]. Since the discovery of the Ziegler-Natta catalysts many attempts have been made to improve the stereospecificity of the catalyst, for example systems including a titanium compound catalyst, a co-catalyst and active MgCl_2 as a support.

2.1.1.2 Metallocene catalysts

Metallocene-based polymerization catalysts are homogeneous, soluble organometallic compounds [5]. They have the basic formula of $\text{Cp}_2\text{MtX}_2/\text{MAO}$, where Mt is a group 4 transition metal (titanium, zirconium or hafnium) centred between two cyclopentadienyl (Cp) groups and X is a chlorine or alkyl group. The Cp groups can be bridged by a one or more carbon or silicon atoms between them. This bridge eliminates the rotation of the Cp groups, which affects the tacticity of the polymer. Methylalumoxane (MAO) acts as a co-catalyst. The stereospecific structure and the

molecular weight of the homopolymer, as well as the co-monomer addition, can be better controlled than with Ziegler-Natta catalysts. Furthermore, metallocene catalysts allow many different co-monomers, such as ethylene, 1-butene, 1-hexene and 1-heptene to be used in the co-polymerization [6].

2.1.2 Polypropylene configurations

The polypropylene chain resulting from the head-to-tail addition of propylene monomers can have three different configurations: the regular isotactic, the regular syndiotactic and the irregular atactic configuration, which are classified based on the arrangement of the methyl groups with regard to the polymer backbone. In the extended isotactic polypropylene chain all methyl groups are on the same side of the plane formed by the main chain carbon atoms. In the syndiotactic polypropylene the methyl groups are arranged alternating on both sides of the plane. In the atactic configuration the methyl groups are placed randomly on both sides along the polymer chain [4]. The three configurations of the polypropylene are illustrated in Figure 2.1.

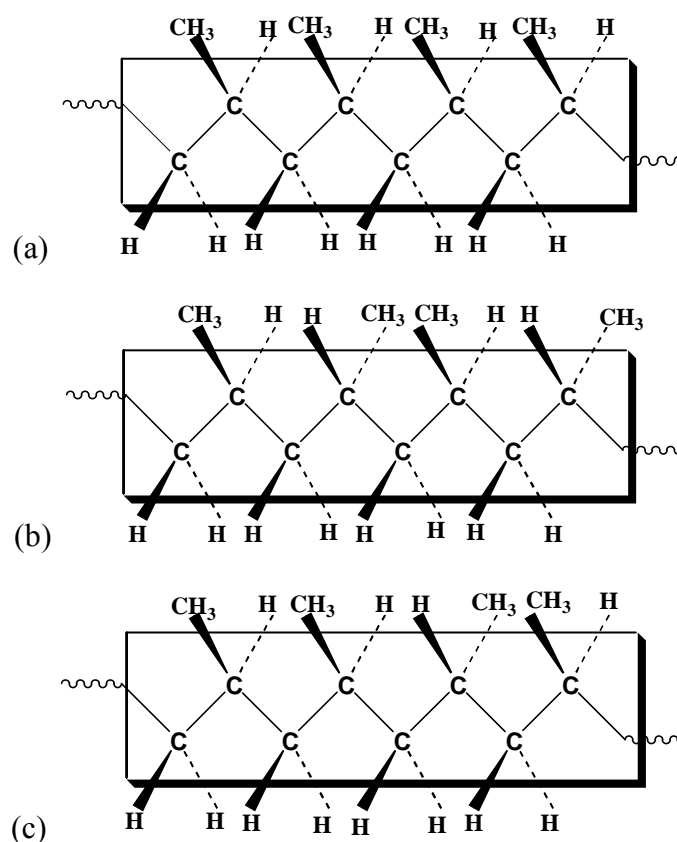


Figure 2. 1: Schematic illustration of the stereochemical configurations of polypropylene: a) isotactic, b) syndiotactic, c) atactic.

2.1.3 Polypropylene conformations and crystal structures

None of the configurations of polypropylene exists in an extended conformation. The chain assumes a helical structure in order to relieve the steric hinderance, which is caused as a result of the presence of methyl groups along the chain backbone, in order to achieve an energy minimum.

The polymer chain of isotactic polypropylene adapts the conformation of a three-folded chain $2 \times 3/1$ helix trans(t)-gauche(g), with a repeat distance of 6.5Å. This conformation leads to the lowest intramolecular interaction energy of the methyl groups attached to the polypropylene chain [7]. The isotactic polypropylene helix exhibits four different chiralities. Both right-handed (R) and left-handed (L) helices are based on the helix direction, which can be up or down, depending on the methyl group orientation. Figure 2.2 illustrates the four possible chain conformations of isotactic polypropylene [8]. Syndiotactic polypropylene exhibits three different chain conformations: the planar zigzag chain (tt), the $(4 \times 2/1)$ helix $(t_2g_2)_2$ and the $(t_6g_2t_2g_2)$ conformation, which is an intermediate between the planar zigzag and the helix form. The helix conformation leads to the lowest interaction energy between the methyl groups [4]. Atactic polypropylene with a random arrangement of the methyl groups along the polymer chain leads to random conformations.

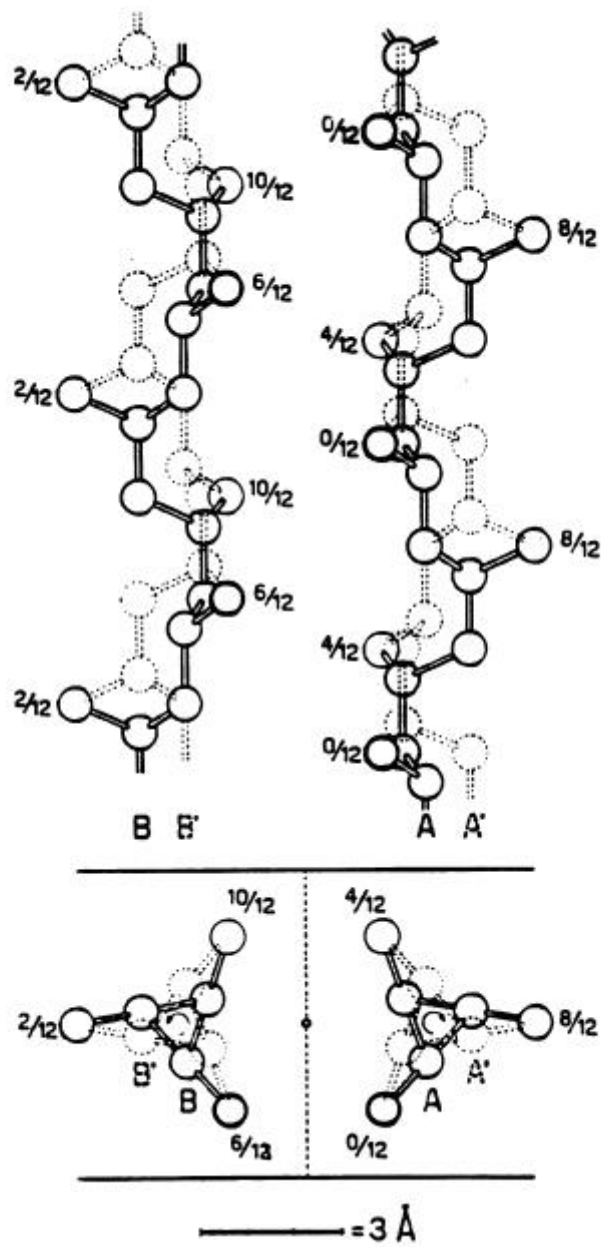


Figure 2. 2: Illustration of the helical structure of isotactic polypropylene: a) right-handed, b) left-handed helices. The continuous line shows the up direction and the dashed line the down direction of the methyl groups [8].

2.1.4 Crystallinity and polymer structure

Both the crystallization behaviour and crystal form of the polymer are strongly affected by the configuration (tacticity) and conformational structure of the polypropylene chain. Isotactic and syndiotactic polypropylene can crystallize. The degree of crystallinity is commonly in the range of 40% to 70% and depends on the level of the tacticity of the polymer [3]. Atactic polypropylene is considered as uncrystallizable, since the chain structure lacks regularity. The syndiotactic

polypropylene chains form either an orthorhombic unit cell if they have a $(t_2g_2)_2$ or a planar zigzag conformation and triclinic unit cell with the $(t_6g_2t_2g_2)$ conformation [4]. Isotactic polypropylene can crystallize in three different crystal forms depending on the polymer structure and the crystallization conditions: the α -form with a monoclinic, the γ -form with an orthorhombic and the β -form with a hexagonal unit cell [9-11].

2.2 The crystalline structure of isotactic polypropylene (iPP)

2.2.1 The α -phase of iPP of isotactic polypropylene

The α -phase is the most common crystalline form of iPP. It is observed for both melt- and solution-crystallized samples prepared under atmospheric pressure.

2.2.1.1 The unit cell of the α -phase

The monoclinic unit cell was first documented by Natta and Corradini [7]. The alternating left-handed (L) and right-handed (R) polymer chains are arranged alternately in the unit cell along the b-axis direction, forming layers parallel to the ac-plane [9], as indicated in Figure 2.3. The location of the methyl groups in both the left or right-handed helices can be positioned 'up' or 'down' (up or dw, see Figure 2.2).

The α -phase can be classified into two types based on the possibility of the chains to be positioned 'up' or 'down'. The first model, by Natta and Corradini [7], assumes an equal statistical distribution of up and down chains, but the L and R helices occupy well defined positions. This is the disordered α_1 -structure with crystallographic symmetry (space group of $C2/c$), as illustrated in Figure 2.3a. In this model the unit cell has the following parameters $a = 6.65 \text{ \AA}$, $b = 20.96 \text{ \AA}$, $c = 6.50 \text{ \AA}$, $\beta = 99.33^\circ$ and $\alpha = \gamma = 90^\circ$. The crystallographic density is 0.936 g/cm^3 . The second model, the well ordered α_2 structure, was proposed later by Mencik [3]. It can be obtained by re-crystallizing or annealing [3, 9], and its structure is shown in Figure 2.3b. It was observed that the crystallographic symmetry of the α_2 form is $P2_1/c$. The unit cell parameters are: $a = 6.65 \text{ \AA}$, $b = 20.96 \text{ \AA}$, $c = 6.5 \text{ \AA}$ [9] and $\beta = 99.62^\circ$. The density at 25°C is 0.946 g/cm^3 [4].

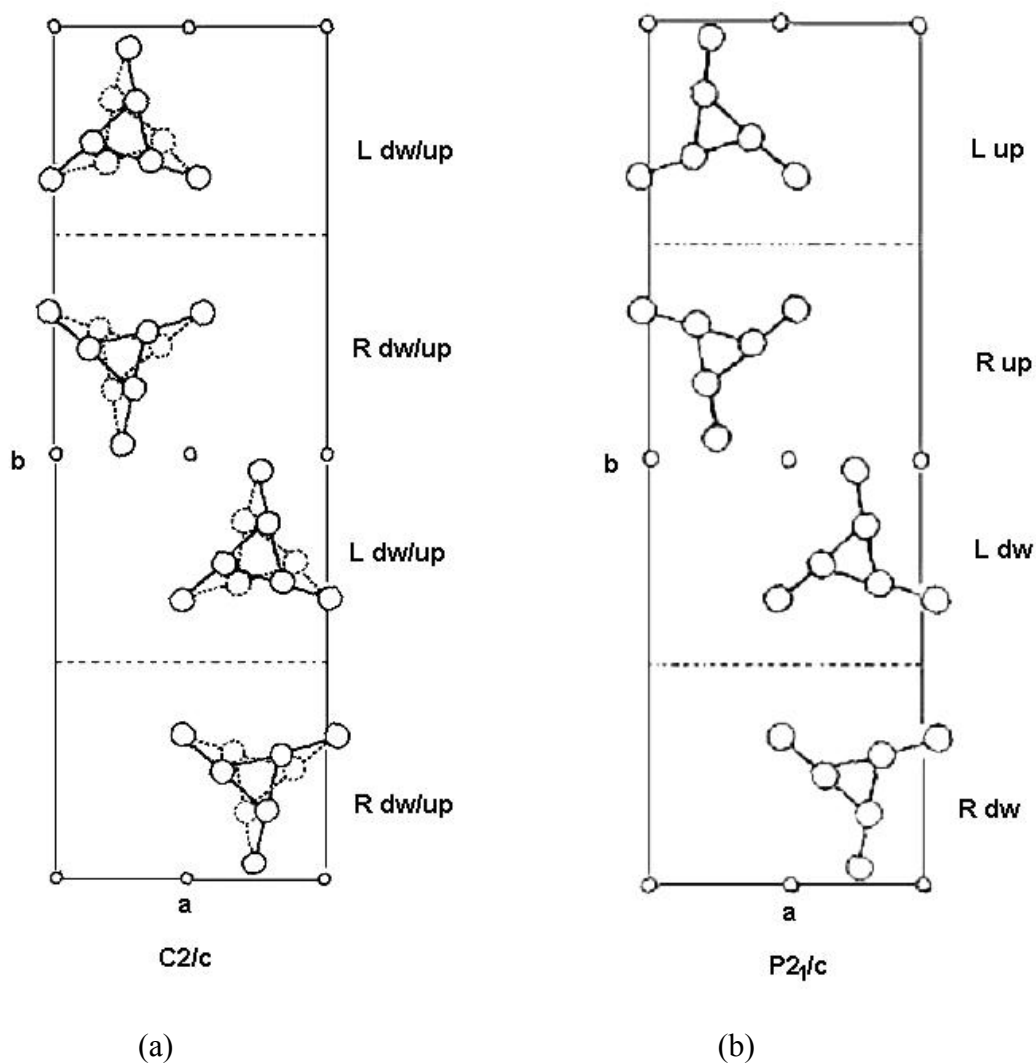


Figure 2. 3: Illustration of the two crystallization types of α -ipp, a) the $\alpha_1(C2/c)$ and b) the $\alpha_2(P2_1/c)$ form [9].

The alteration of right and left handed helices along the b-axis leads to two different possible surface structures of the a-c (010) plane: a four-face pattern when one methyl group is exposed and a five-face pattern when two methyl groups are exposed along the $\pm b$ axis direction. Stocker et al. [12] proposed that the four-face pattern is preferred if the iPP is epitaxially crystallized on benzoic or nicotinic acid substrates, whereas alkali-halide as substrates result predominately in a five face pattern. In their experiments they first crystallized the iPP epitaxially on the substrate, and then dissolved the substrate with ethanol. Finally, the methyl groups of the contact surface were visualized with AFM. Both possible patterns are schematically shown in Figure 2.4 [13].

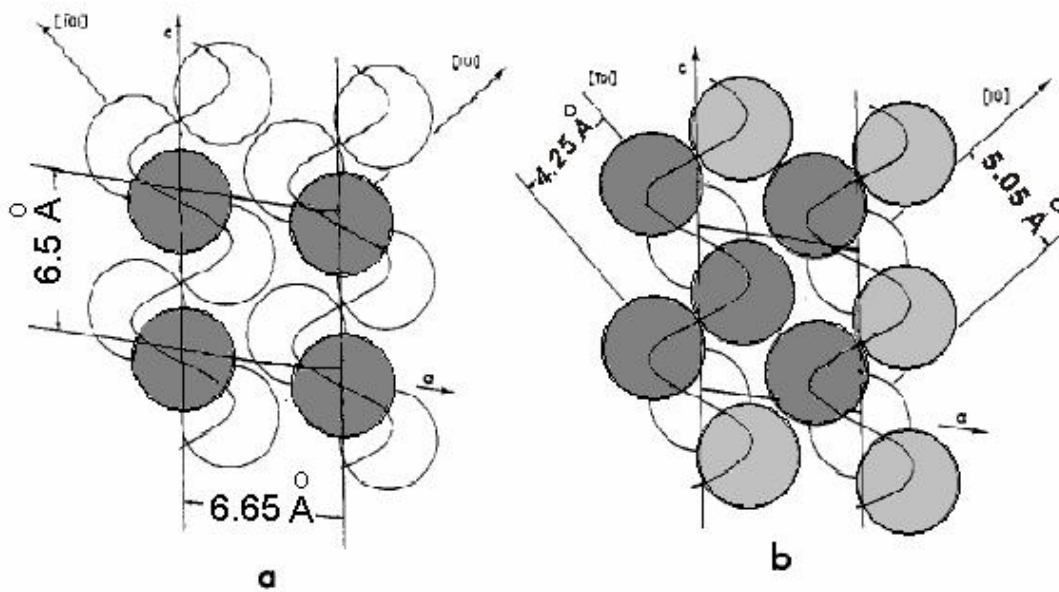


Figure 2. 4: Schematic illustration of the two possible surface structures of the a-c (010) plane of α -iPP, a) four-face pattern, b) five-face pattern [14].

The value of the thermodynamic equilibrium melting point, T_m° , of the α -phase has been studied by many researchers [9]. T_m° was found to be between 185°C and 209°C. The variation of T_m° is related to the different techniques used to measure it. The results of the heat of fusion (ΔH_f°) measurements are also scattered. Data obtained from calorimetry show values around $\Delta H_f^{\circ} = 8.7 \pm 0.8$ kJ/mol, while the value obtained with the method of the melting point depression by diluents is $\Delta H_f^{\circ} = 9.1 \pm 1.6$ kJ/mol. Recently, a value of $\Delta H_f^{\circ} = 8.7$ kJ/mol was adopted [9].

2.2.1.2 The lamellar structure of the α -phase

The most common structural feature of melt crystallized iPP is the lamellar crystallite. Polymer chains in the α -form of isotactic polypropylene form a helical structure in a monoclinic unit cell and fold into lamellae with thicknesses of 50–200 Å [9]. In the α -phase of iPP, the polymer chains are oriented normal (in c-direction) to the ab-plane of the crystals. Radial growth of lamellae is dominant. The lamellae can, however, also associate tangentially, with the tangential lamella branching off with an 80° or 100° angle from the ac plane of the radial lamellae. This forms a cross-hatched structure within the lamellae, which aggregate to form spherulites [14]. This

morphology feature is illustrated schematically in Figure 2.5.

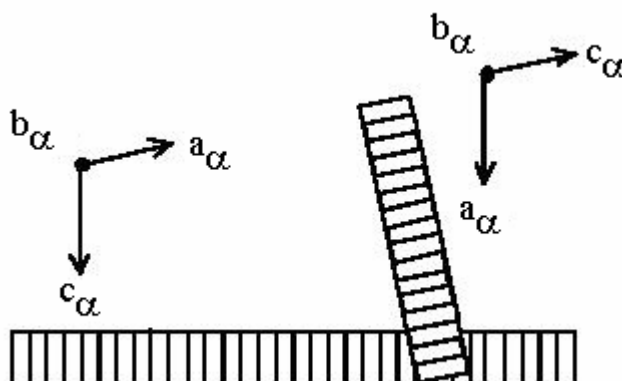


Figure 2. 5: Schematic illustration of α -iPP lamellae branching (cross-hatched structure) from [15].

As indicated in Figure 2.5, the preferred growth direction of the dominant radial lamellae has been determined to be the a direction, with the chain axis (c-axis) nearly normal to the radial direction. It has been proposed that the 80° or 100° branching angle corresponds to the matching of the a- and c-axis pair in the radial lamellae with the c- and a-axis of the tangential lamellae [14, 15]. It has also been proposed that branching occurs whenever two successive a-c layers are made of the same hand, as for example LRLRRLR or LRLRL, whereas the crystallographic unit cell requires that they are of opposite hand LRLRLR [16].

2.2.1.3 The spherulite structure of the α -phase

The α -form spherulite of i-PP is the primary form polypropylene assumes under normal processing conditions. Three different types of spherulites were proposed by Padden and Keith in 1959 [17] for the α -phase, based on their optical properties. The classification is determined by their birefringence: positive (α I), negative (α II), and mixed spherulites [17-20]. Both negative and positive birefringent spherulites show a Maltese cross pattern under crossed polarizers. α I is formed below 134°C and the positive birefringence is due to spherulites with predominantly tangential lamellae, which are lost at 160 - 170°C . α II is formed above 137°C , with negative birefringence,

resulting from spherulites, in which radial lamellae are dominant [21]. In spherulites with mixed birefringence regions, which show positive, negative and no birefringence, the lamellae are randomly distributed and no Maltese cross can be observed. The cross-hatching phenomenon, which is responsible for the differences in birefringence of α -spherulites, can be explained by an initial radial ‘mother’ lamellae crystallization, followed by a tangential ‘daughter’ lamellae crystallization. These can grow homo-epitaxially on the lateral (010) plane, which results in an interchange of a- and c-axes orientation in the mother and daughter lamellae across the contact plane, while the b-axis orientation is preserved [14]. The birefringence changes from positive to negative with increasing crystallization temperature, as the tangential lamellae undergo premelting [9]. Increasing the tacticity decreases the formation of tangential lamellae further and nearly 100% α II form can be obtained with a very stereoregular isotactic polypropylene [4]. Optical micrographs of both α I and α II iPP spherulites are shown in Figure 2.6.

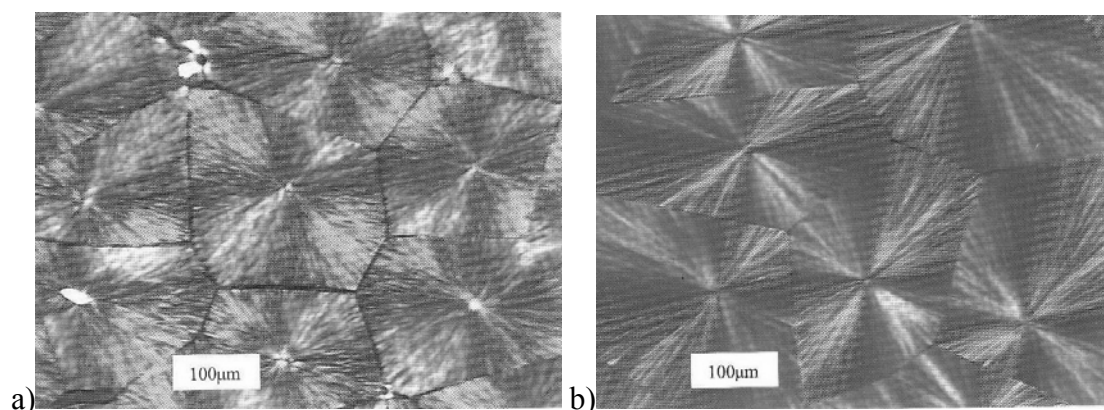


Figure 2. 6: Optical micrograph of α -iPP spherulites, a) type I crystallized at 130°C, b) type II crystallized at 140°C [22].

2.2.2 The β -phase of isotactic polypropylene

The β -form of isotactic polypropylene was first reported by Padden and Keith in 1959 [17]. The preparation of high percentage or pure β -phase can be accomplished under special conditions, such as isothermal crystallization at relatively low temperatures, or the use of a β -nucleating agent like calcium stearate, under a temperature gradient or under shear [23].

2.2.2.1 The unit cell of the β -phase

There have been many attempts to determine the unit cell of the β -phase, based on X-ray diffraction measurements. Finally a hexagonal lattice was proposed by Turner-Jones and Cobbold [14] with the following parameters: $a = b = 19 \text{ \AA}$, $c = 6.5 \text{ \AA}$, $\gamma = 120^\circ$. Recently a trigonal unit-cell, containing three isochiral helices, was documented for the β -phase with the lattice parameters $a = b = 11.01 \text{ \AA}$, $c = 6.5 \text{ \AA}$, $\beta = 120^\circ$ and $\alpha = \beta = 90^\circ$ [14, 24-27]. The β -phase has a density of 0.92 g/cm^3 . The thermodynamic properties of the β -phase have not been as comprehensively studied, as those of the α -phase. The β -phase is metastable relative to the α -phase ($T_m \cong 155^\circ\text{C}$ versus 180°C). The equilibrium melting temperature of the crystals (T_m^0) ranges from 170°C to 200°C [4]. The values of ΔH_f^0 vary from 4.76 kJ/mol to 7.45 kJ/mol [3, 4].

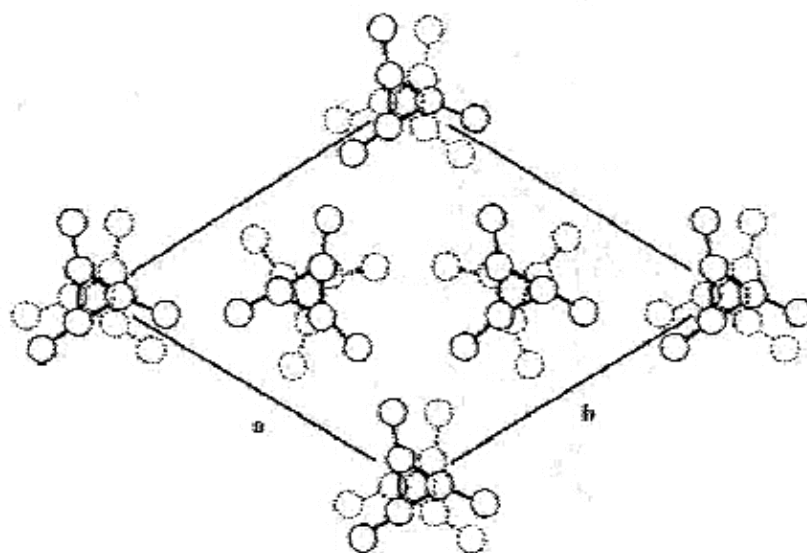


Figure 2. 7: Schematic representation of the arrangement of iPP-helices in the β -phase. The lines indicate the a- and b-axes; the c-axis is perpendicular to the plane of view [28].

2.2.2.2 The lamellar structure of the β -phase

The parallel, stacked lamellae of β -spherulites follow the general characteristics of spherulitic growth in semi-crystalline materials and the cross-hatching phenomenon of the α -lamellae is absent. The radial growth direction of the lamellae has been reported to be along the crystallographic a-axis of the unit cell [19].

2.2.2.3 The spherulite structure of the β -phase

β -spherulites can be divided into two types: the strong, negatively birefringent, radial β III type and the β IV type, which is characterized by negative birefringence as well as banded concentric rings, as shown in Figure 2.8. The concentric banding of the β IV type has been associated with a periodic orientation of the lamellae along the radial direction of the spherulite, whereas the β III type has been associated with a random orientation [3]. The formation temperature of the β III type is below 142°C and for the β IV type between 126°C and 132°C, as reported by Norton and Keller [19, 20]. The growth-rate of β -spherulites is up to 70% faster than for α -spherulites in temperature ranges of 105°C-141°C. Outside this temperature range the growth rate of α -spherulites is faster [14]. The parallel stacked lamellae of β -spherulites do not show any cross-hatching. Lamellae have been observed to form sheaf-like spherulitic structures with interconnected boundaries, which is different from the distinct boundaries of α -spherulites.

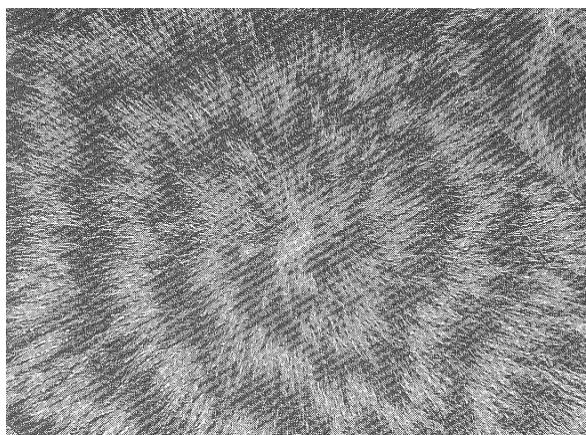


Figure 2. 8: SEM micrograph of an etched banded β -spherulite type β IV crystallized at 130°C [29].

2.2.3 The γ -phase of isotactic polypropylene

The γ -phase was first observed by Addink and Beitema in 1961 [9]. It typically coexists with the α -phase, although nearly pure γ -phase iPP has been observed [30].

The nearly pure γ -phase can be obtained by using low molecular weight ($MW \cong 1000$ - 3000) isotactic polypropylene [12], high molecular weight iPP, which is crystallized under high pressures [31] or isotactic polypropylene with small amounts (4-10%) of comonomer (ethylene, 1-butene or 1-hexene) [32-35]. It can also be prepared under atmospheric pressure using isotactic polypropylene with low tacticity or made by homogeneous metallocene catalysts [36-41].

2.2.3.1 The unit cell of the γ -phase

Based on x-ray diffractions a triclinic unit cell was first proposed for the γ -phase [9]. Recently, Brückner and Meille [42] proposed that the triclinic unit cell can be considered as a sub-cell of a face-centred, orthorhombic unit cell with the parameters $a = 8.54 \text{ \AA}$, $b = 9.93 \text{ \AA}$, and $c = 42.41 \text{ \AA}$. The structure is made up of bilayers, which are tilted 80° or 100° to each other rather than being parallel. Each bilayer is composed of one (R) and one (L) handed helix, and the overall sequence along the c-axis is LLRLLRR. In this unit cell the c-axis is not parallel with the chain axis direction [24, 30, 43]. The γ -phase unit cell is shown in Figure 2.9 [43].

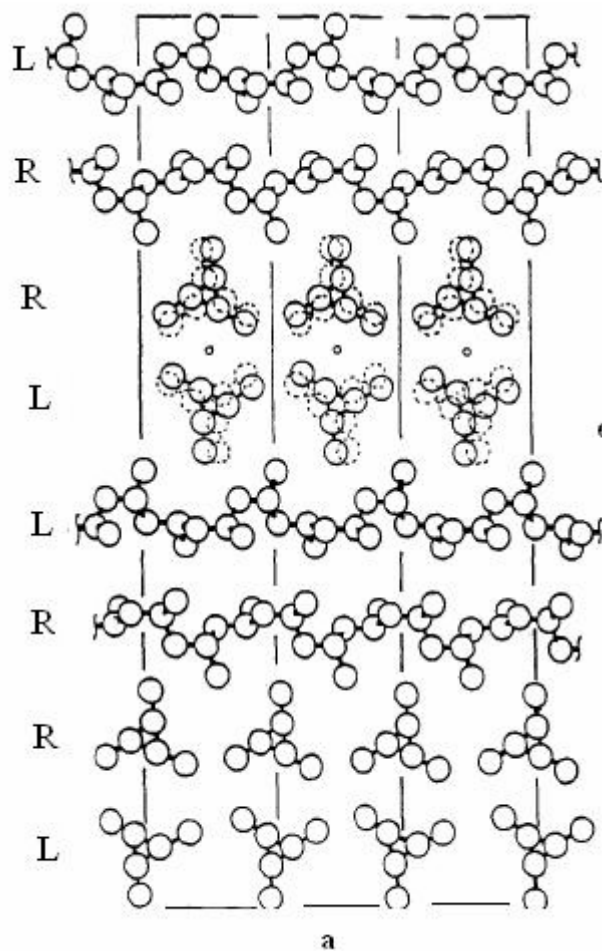


Figure 2. 9: Schematic representation of the arrangement of iPP-helices in the γ -phase [43].

Using AFM Stocker et al. [12] revealed the methyl groups of the contact face of γ -phase iPP crystallized epitaxially on benzoic or nicotinic acid substrates. They demonstrated that the a-b (010) plane with a four-face pattern of the methyl groups is preferred, and that the five-face pattern dominates when alkali halides are used as substrates. The chain axis is tilted 40° to the lamellar surface in the γ -phase. Thomann et al. [44] reported that AFM analysis on a molecular scale of thin iPP films prepared from solution reveals the methyl groups of the a-c (110) plane of the γ -phase iPP. The a-c plane of the γ -phase is schematically illustrated in Figure 2.10.

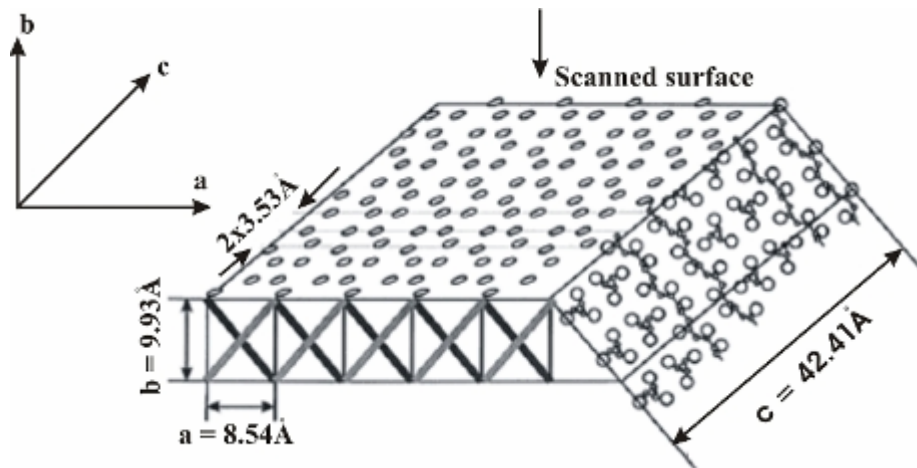


Figure 2. 10: Schematic illustration of the crystal lattice with dimensions and the arrangement of helices in the a-c (110) plane of the γ -phase [44].

The value of the thermodynamic equilibrium melting point, T_m^0 , of the γ -phase is 187.2 °C and the value of the heat of fusion $\Delta H_f^0 = 6.1$ kJ/mol [9, 45].

2.2.3.2 The lamellar structure of the γ -phase

The polymer chains of the γ -phase are tilted $\pm 40^\circ$ to the normal direction of the lamellae. The γ -phase lamellae grow epitaxially with an angle of 40° on α -phase lamellae, analogous to the homo-epitaxial growth of secondary lamellae (cross-hatches) in the α -phase [9]. Figure 2.11 illustrates this arrangement schematically. The explanation of the γ - α branching, based on electron diffraction microscopy, proposes that the γ -phase could nucleate on the 010 face of the α -phase in thin films [12, 16].

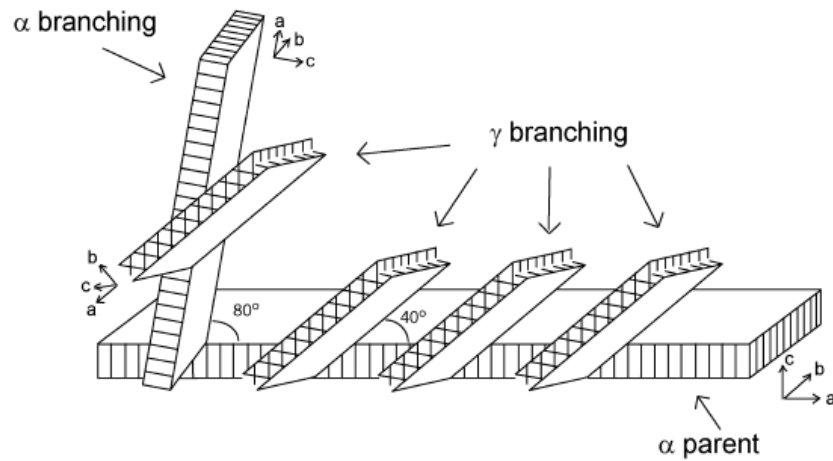


Figure 2. 11: Schematic illustration of the γ - α branching [46].

In addition to the γ - α lamellae epitaxially growth, the homo-epitaxially growth of γ -lamellae onto γ -lamellae, which result in a feather-like structure, was proposed by Mezghani and Phillips [31]. This structure was obtained for samples prepared under a pressure of 200 MPa and the γ - γ lamellae branching-angle is about 140° .

2.2.3.3 The spherulite structure of the γ -phase

The γ -phase is frequently connected with the α -phase [43, 47], although pure single crystals of the γ -phase were also reported [30, 31]. There have not been as many studies on pure γ -spherulites as of α -spherulites. Mezghani and Phillips [31, 48] reported the different types of γ -iPP spherulites crystallized at 200 MPa in a temperature range of 176 - 206°C based on their optical properties. A negative birefringence type, γ_n , resulted from melt crystallization in a temperature range of 187 - 198°C . A positive type, γ_p , was obtained above 199°C and below 184°C . A mixed birefringence, γ_m , was observed in the range of 180 - 187°C and 192 - 199°C . The positive type, γ_p , can be explained by the feather-like structure as shown in Figures 2.12 and 2.13. The negative birefringence type, γ_n , is related to radial lamellae growth. A mixture of both feather-like and radial types results in mixed type of birefringence [31].



Figure 2. 12: Reflection optical micrograph of lamellae in iPP crystallized at 200 MPa and an isothermal crystallization temperature of 203°C. Lamellae are arranged in the form of feathers. The sample was etched with permanganate potassium for 30 minutes [31].

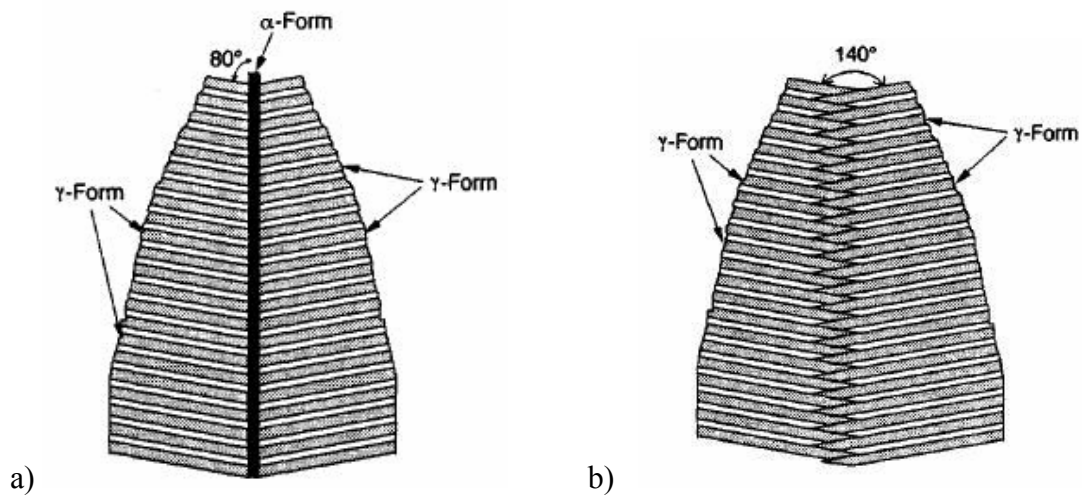


Figure 2. 13: a) Epitaxial growth of γ -lamellae on α -lamellae, b) epitaxial growth of γ lamellae on γ -lamellae [31].

The γ -spherulite structure of iPP samples prepared with metallocene catalysts has been studied by Thomann et al. [44]. The polarized light micrographs of these samples are shown in Figure 2.14. They proposed that the micrograph taken after a crystallization time of 1:50 h at a crystallization temperature of 120°C shows elongated entities that are distinctive for the early stage of α -phase lamellae with a γ -phase ongrowth similar to that reported for low molecular weight samples. The micrograph taken after 4:30 h shows more bundle-like entities. The micrographs taken

after 23 and 43 h do not show any significant difference, indicating that the growth of the bundle-like entities is finished long before the bundles become space filling. After this time, only diffuse structures between the needle-like entities appear which are not visible in the polarized light micrographs. This sample crystallized entirely in the γ -modification, without any contributions of the α -form.

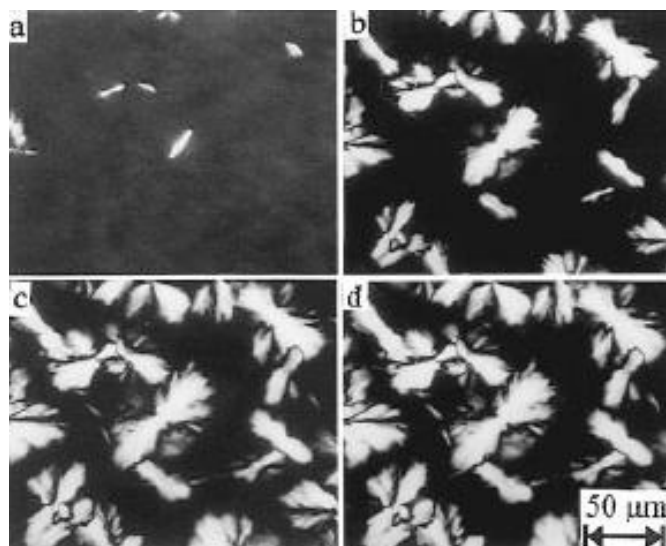


Figure 2. 14: Polarized light micrographs taken during isothermal crystallization of metalocene iPP at 120°C after crystallization times of: a) 1:50 h, b) 4:30 h, c) 23 h and d) 43 h [44].

2.2.4 Mesomorphic (smectic) phase of isotactic polypropylene

When isotactic polypropylene is rapidly quenched from the melt, it results in an intermediate phase between the well ordered crystalline and the disordered amorphous phases being formed. This phase is metastable and changes into the α -phase with annealing above 70°C [3]. Polymer chains have been shown to form helical structures, but the unit cell and lamellar structures have not yet been resolved [4]. Some studies suggested that this form may be a para-crystalline phase, resulting from deformed or distorted lattice structures. Other experiments indicate a lack of lamellar order in addition to a low density and small size of ordered structures. These characteristics result in high clarity, which is useful in quenched films [9].

2.3 Polypropylene copolymers

Although homo-polypropylene exhibits excellent properties for many applications, such as films, pipes and fibres, it is brittle at low temperatures due to its glass transition temperature, which is about 0°C. It can, however, be copolymerized with other α -olefins, in order to obtain more flexible and high impact products. The copolymerization can be classified into the random (statistical) copolymerization and the block (sequential) copolymerization.

2.3.1 Random copolymers

Random, also known as statistical copolymers, can be obtained by the copolymerization of propylene monomer and 2 – 7 wt % of another 1-olefin as comonomer, such as ethylene, butene or hexene [49]. This leads to the introduction of the 1-olefin comonomer into the main chain, which decreases the overall crystallinity, provides a broader softening range with a reduced melting point, increases the fraction of soluble polymer, and improves the clarity and surface gloss. The improvements of these properties are dependent on the amount of comonomer and its distribution along the chain. The distribution of the comonomer among the polymer chain is controlled by the type of the catalyst. Typically, Ziegler-Natta catalysts produce polymers with a non-uniform distribution of the comonomer units, which results in a major crystallizable fraction with long sequence of un-interrupted polypropylene chains and a minor uncrystallizable fraction with high 1-olefin content. The resulting polymer crystallizes mainly in the α -phase of isotactic polypropylene. In the case of Metallocene catalysts, the polymer has a very uniform distribution of comonomer units along the polypropylene chain, which encourages the formation of the γ -phase of isotactic polypropylene.

2.3.2 Impact (block) copolymers

The impact resistance of polypropylene can be increased by blending with various ethylene-propylene (EP) copolymer rubbers (physical blend). Another method consists of producing an elastomeric EP phase in situ during the polymerization (reactor blend). This requires a two stage process. Firstly, homo-polypropylene is prepared, secondly, a mixed monomer feed of ethylene and propene is added to obtain

a largely amorphous elastomeric phase within the polymer particles [50]. This results in a product with the copolymer sequence ranging from polypropylene-like to polyethylene-like molecules. The overall morphology presents polypropylene as matrix, in which elastomer particles with diameters in the range between 0.5 - 3 μm are dispersed [51]. The elastomer particles (rubber phase) provide good toughness [52], while the homopolymer matrix gives excellent high-temperature performance and stiffness.

2.4 References

1. J. Huang, G. L. Rempel. *Ziegler-Natta catalysts for olefin polymerization: mechanistic insights from metallo systems*. Progress in Polymer Science. 1995, **20**, 459-526.
2. K. Soga, T. Shiono. *Ziegler-Natta catalysts for olefin polymerization*. Progress in Polymer Science. 1997, **22**, 1503-1546.
3. Jr. Edward, P. Moore. *Polypropylene Handbook*. 1st ed. Vol. 1. Munich Vienna New York: Carl Hanser Verlag. 1996, 11-73.
4. J. Karger-Kocsis. *Polypropylene structure, blends and composites*. 1st ed. Vol. 1. London: CHAPMAN & HALL. 1995, 3-50.
5. Y. Imanishi, N. Naga. *Recent developments in olefin polymerization with transition metal catalysts*. Progress in Polymer Science. 2001, **26**, 1147-1198.
6. L. Resconi, L. Cavallo, A. Fait, F. Piemontesi. *Selectivity in propene polymerization with metallocene catalysts*. Chemical Reviews 2000, **100**, 1253-1345.
7. P. Corradini G. Natta. *Structure and properties of isotactic polypropylene*. Nuovo Cimento. 1960, **1**, 40-51.
8. V. Busico, R. Cipullo. *Microstructure of polypropylene*. Progress in Polymer Science. 2001, **26**, 443-433.
9. S. Brückner, S. V. Meille, V. Petraccone, B. Pirozzi. *Polymorphism of isotactic polypropylene*. Progress in Polymer Science. 1991, **16**, 361-404.
10. B. Lotz. *What can polymer crystal structure tell about polymer crystallization processes?* The European Physical Journal E. 2000, **3**, 185–194.
11. F. C. Tsai J. H. Chen, Y. H. Nien, P. H. Yeh. *Isothermal crystallization of isotactic polypropylene blended with low molecular weight atactic polypropylene. Part I. Thermal properties and morphology development*. Polymer. 2005, **46**, 5680-5688.
12. W. Stocker, S. N. Magonov, H. J. Cantow, J. C. Wittmann, B. Lotz. *Contact faces of epitaxially crystallized α - and γ -phase isotactic polypropylene observed by atomic force microscopy*. Macromolecules. 1993, **26**, 5915-5923.
13. C. Mathieu, A. Thierry, J. C. Wittmann, B. Lotz. *“Multiple” nucleation of the (010) contact face of isotactic polypropylene, a phase*. Polymer. 2000, **41**,

7241-7253.

14. B. Lotz, C. Wittmann, A. J. Lovinger. *Structure and morphology of poly(propylenes): a molecular analysis*. Polymer. 1996, **22**, 4979-4992.
15. I. Masada, T. Okihara, S. Murakami, M. Ohara, A. Kawaguchi, K. Katayama. *A bimodal structure of solution-grown isotactic polypropylene with orthogonally crossed lamellae*. Journal of Polymer Science Part B: Polymer Physics. 1993, **31**, 843-852.
16. B. Lotz, J. C. Wittmann. *The molecular origin of lamellar branching in the α (monoclinic) form of isotactic polypropylene*. Journal of Polymer Science Part B: Polymer Physics. 1986, **24**, 1541-1558.
17. F. J. Padden, J. D. Keith. *Spherulitic crystallization in polypropylene*. Journal of Applied Physics. 1959, **30**, 1479-1484.
18. A. Pawlak, E. Piorkowska. *Crystallization of isotactic polypropylene in a temperature gradient*. Colloid Polymer Science. 2001, **279**, 939-946.
19. D. R. Norton, A. Keller. *The spherulitic and lamellar morphology of melt-crystallized isotactic polypropylene*. Polymer. 1985, **26**, 704-716.
20. J. G. Liua J. J. Zhoua, S. K. Yana, J. Y. Donga, L. Lia, C. M. Chanb, J. M. Schultzc. *Atomic force microscopy study of the lamellar growth of isotactic polypropylene*. Polymer. 2005, **In Press**, 1-11.
21. R. H. Olley, D. C. Bassett. *On the development of polypropylene spherulites*. Polymer. 1989, **30**, 399-409.
22. Jr. Edward, P. Moore. *Polypropylene Handbook*. 1st ed. Vol. 1. Munich Vienna New York: Carl Hanser Verlag. 1996, 113-176.
23. A. Romankiewicz, T. Sterzynski, W. Brostow. *Structural characterization of α - and β -nucleated isotactic polypropylene*. Polymer International. 2004, **53**, 2086-2091.
24. D. R. Ferro S. V. Meille, S. Brückner, A. J. Lovinger, and F. J. Padden. *Structure of β -isotactic polypropylene: A long-standing structural puzzle*. Macromolecules. 1994, **27**, 2615-2622.
25. D. C. Martin W. Xu, E. M. Arrunda. *Finite strain response, microstructural evolution and β - α phase transformation of crystalline isotactic polypropylene*. Polymer. 2005, **46**, 455-470.
26. W. Stocker, M. Schumacher, S. Graff, A. Thierry, J. C. Wittmann, B. Lotz.

- Epitaxial crystallization and AFM investigation of a frustrated polymer structure: isotactic poly(propylene), β -phase.* *Macromolecules.* 1998, **31**, 807-814.
27. J. Varga D. Trifonova, G. J. Vancso. *AFM study of lamellar thickness distributions in high temperature melt-crystallization of β -polypropylene.* *Polymer Bulletin.* 1998, **41**, 341–348.
 28. S. Brückner and SV. Meille. *Polymorphism in crystalline polypropylene*, in *polypropylene an A-Z Reference*, J. Karger-Kocsis, Editor. Dordrecht: Kluwer Academic Publishers. 1999, 606-614.
 29. D. T. Haeringen, J. Varga, G. W. Ehrenstein, G. J. Vancso. *Features of the hedritic morphology of β -isotactic polypropylene studied by atomic force microscopy.* *Journal of Polymer Science Part B: Polymer Physics.* 2000, **38**, 672-681.
 30. J. R. Isasi, L. Mandelkern, M. J. Galante, R. G. Alamo. *The Degree of crystallinity of monoclinic isotactic poly(propylene).* *Journal of Polymer Science Part B: Polymer Physics.* 1999, **57**, 323-334.
 31. K. Mezghani, P. J. Phillips. *The γ -phase of high molecular weight isotactic polypropylene. II: The morphology of the γ -form crystallized at 200MPa.* *Polymer.* 1997, **38**, 5725-5733.
 32. K. Mezghani, P. J. Phillips. *γ -Phase in polypropylene copolymers at atmospheric pressure.* *Polymer.* 1995, **36**, 2407-2411.
 33. I. L. Hosier, R. G. Alamo, J. S. Lin. *Lamellar morphology of random metallocene propylene copolymers studied by atomic force microscopy.* *Polymer.* 2004, **45**, 3441–3455.
 34. S. Piccarolo T. Foresta, G. Goldbeck-Wood. *Competition between α and γ phases in isotactic polypropylene: effects of ethylene content and nucleating agents at different cooling rates.* *Polymer.* 2001, **42**, 1167-1176.
 35. Y. Feng, X. Jin, J. N. Hay. *Crystalline structure of propylene–ethylene copolymer fractions.* *Journal of Applied Polymer Science.* 1998, **68**, 381–386.
 36. R. G. Alamo. *The Role of Defect microstructure in the crystallization behaviour of Metallocene and $MgCl_2$ -Supported Ziegler-Natta isotactic poly(Propylenes).* *Polímeros: Ciência e Tecnologia.* 2003, **13**, 270-275.
 37. F. X. Guan J. T. Xu, T. Yasin, Z. Q. Fan. *Isothermal crystallization of*

- Metallocene-based polypropylenes with different isotacticity and regioregularity.* Journal of Applied Polymer Science. 2003, **90**, 3215-3221.
38. R. Thomann, H. Semke, R. D. Maier, Y. Thomann, J. Scherble, R. Mulhaupt, J. Kressler. *Influence of stereoirregularities on the formation of the γ -phase in isotactic polypropene.* Polymer. 2001, **42** 4597-4603.
 39. C. De Rosa F. Auriemma. *Crystallization of Metallocene-made isotactic Polypropylene: Disordered Modifications Intermediate between the α - and γ -forms.* Macromolecules. 2002, **35**, 9057-9068.
 40. C. De Rosa, F. Auriemma, C. Spera, G. Talarico, M. Gahleitner. *Crystallization properties of elastomeric polypropylene from alumina-supported tetraalkyl zirconium catalysts.* Polymer. 2004, **45**, 5875-5888.
 41. F. Auriemma C. D. Rosa, T. C. Longo, A. C. Boccia. *Stereoblock polypropylene from a Metallocene catalyst with a Hapto-Flexible Naphthyl-Indenyl ligand.* Macromolecules. 2003, **36**, 3465-3474.
 42. *The γ -phase of high molecular weight isotactic polypropylene. II: The morphology of the γ -form crystallized at 200 M Pa.* polymer.
 43. S. V. Meille, S. Brückner, W. Porzio. *γ -Isotactic Polypropylene. A structure with nonparallel chain axes.* Macromolecules. 1990, **23**, 4114-4121.
 44. R. Thomann, C. Wang, J. Kressler, R. Muelhaupt. *On the γ -phase of isotactic polypropylene.* Macromolecules. 1996, **29**, 8425-8434.
 45. P. J. Phillips K. Mezghani. *The γ -phase of high molecular weight isotactic polypropylene: III. The equilibrium melting point and the phase diagram.* Polymer. 1998, **39**, 3737-3744.
 46. I. L. Hosier, R. G. Alamo, P. Estes, J. R. Isasi, L. Mandelkern. *Formation of the α and γ polymorphs in random Metallocene propylene copolymers. Effect of concentration and type of comonomer.* Macromolecules. 2003, **36**, 5623-5636.
 47. S. V. Meille, P. J. Phillips, K. Mezghani. *α - γ Disorder in isotactic polypropylene crystallized under high pressure.* Macromolecules. 1996, **29**, 795-797.
 48. K. Mezghani, R. A. Campbell, P. J. Phillips. *Lamellar thickening and the equilibrium melting point of polypropylene.* Macromolecules. 1994, **27**, 997-1002.

49. *Industrial Polymer Handbook*. First ed, ed. S. Edwards. Vol. 4. 2001: Wiley. 692-715.
50. B. Nysten E. Tomasetti, P. G. Rouxhet, C. Poleunis, P. Bertrand and R. Legras. *Surface characterization of polypropylene/(ethylene-propylene) copolymer blends (PP/EP): Application to injection-moulded systems*. *Surface and Interface Analysis*. 1999, **27**, 735-742.
51. R. H. Olley X. Zhang, B. Huang, D. C. Bassett. *Characterization of polypropylene/ethylene copolymers sequentially polymerized with D-TiCl₃/Et₂AlCl_c Catalyst system*. *Polymer International*. 1997, **43**, 45-54.
52. D. W. M. Marr K. Swaminathan. *Morphology characterization of high-impact resistant polypropylene using AFM and SALS*. *Journal of Applied Polymer Science*. 2000, **78**, 452-457.

3 Instrumentation

3.1 Atomic force microscopy (AFM)

Atomic force microscopy (AFM) is one of the most powerful techniques for surface analysis. It is a member of the family of scanning probe microscopes. AFM can be used to study a wide variety of material surfaces, ranging from coatings, ceramics, composites, glasses, synthetic and biological membranes, metals, polymers, to semiconductors. The AFM can be used to study properties such as abrasion, adhesion, corrosion, etching, friction, lubrication, plating, and polishing. AFM is a rich information technique, which provides images of the surface topography and morphology on a nanometre scale [1-3]. The atomic force microscope was developed by Binnig et al. in 1986 [3]. This invention was the result of the need to use scanning tunneling microscope (STM), which is based on the measurement of a tunneling current between a conductive tip and a conductive surface [1, 3, 4], for non-conductive materials. AFM can generate images of the sample surface in ambient conditions as well as under a layer of liquid.

3.1.1 AFM operation

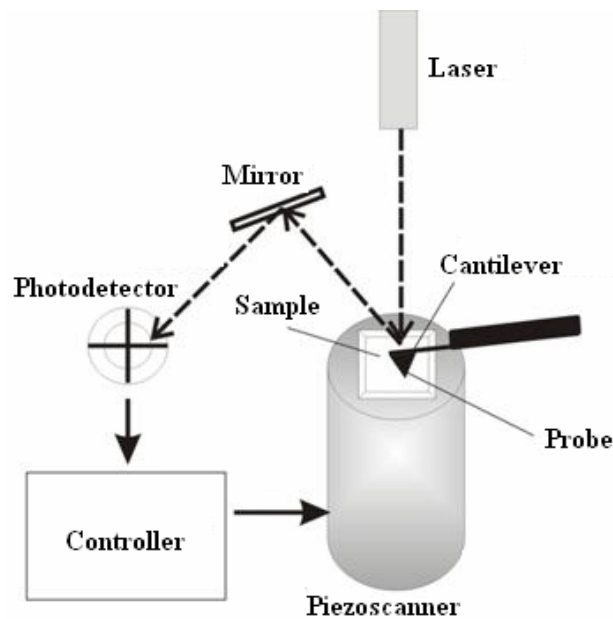


Figure 3. 1: Schematic illustration of the atomic force microscope, showing the probe, cantilever, photodetector, scanner, computer control, and sample.

In order to obtain a topographical image on a molecular level, very small interaction forces at very small distances are measured. These forces, mostly van der Waals forces, are typically in the nano-Newton range, and provide information on the material properties, such as stiffness and adhesion in addition to the topography of the surface [5, 6].

The operation of the AFM is very simple. A fine tip is raster scanned across a surface with a feedback control that enables the determination of interatomic forces acting between the tip and the sample surface. A topographical image is acquired by keeping this force at a constant value. The tips are mainly manufactured from silicon nitride (Si_3N_4) or silicon (Si), and mounted on the end of a soft cantilever. A laser beam is focused onto the back of this cantilever and reflected by a mirror into a segmented photo detector. As the tip senses the surface of the sample, moving up and down, as it follows the surface features depending on the attractive or repulsive forces, the voltage measured in the photodetector varies. If, for example, the probe approaches the surface, the cantilever bends away from the sample because of the repulsive force between the electrons of the surface atoms and the probe, which prevail the attractive van der Waals forces. Since the AFM is based on the determination of forces between the tip and sample, measuring these forces is the key to imaging the sample surface [7].

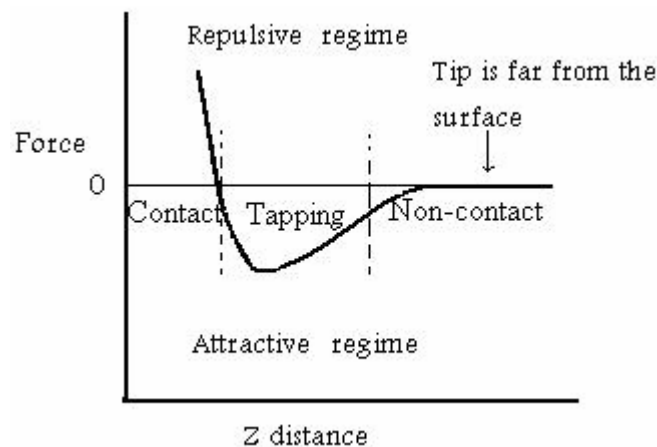


Figure 3. 2: Schematic illustration of the interatomic forces acting between tip/sample atoms for contact, non-contact and tapping mode imaging.

3.1.2 AFM operation modes

Various AFM modes have been developed for special applications. The commonly used modes are: contact mode and non-contact, or tapping mode.

3.1.2.1 Contact mode

In contact mode [5, 8], as the name suggests, the tip follows the sample in direct contact with the surface. The repulsive force acting between the tip and the sample is in the order of 10^{-9} Newton. Since this force is weak, no damage to the surface can be observed unless higher forces are used.

During imaging of the surface, by scanning the tip across the sample, the cantilever is deflected by this repulsive force, according to the changes in topography. The cantilever deflection is measured and compared to a given set point by the control electronics. If this value is not equal to 0, the feedback system applies a voltage to the z-piezo until the set point deflection is obtained again. The voltage that is applied to the z-piezo by the feedback system can be converted directly into height information in nanometer. The main problem of contact mode is the substantial frictional force, as the tip scans across the sample. These frictional forces might cause damage to the sample surface or rearrange loose surface structures.

3.1.2.2 Non-contact mode

In the non-contact mode the AFM is typically operating in the attractive force range to avoid any damage to the sample that might occur in contact mode [8-10]. Attractive forces are mainly van der Waals forces and capillary forces. The tip is oscillated at its resonance frequency above the sample surface. A change in topography results in a change in amplitude or resonance frequency of the oscillating cantilever, which is detected by the feedback system. Again the control system applies a voltage to the z-piezo to obtain the set-point amplitude. This voltage is then converted into a topography image. Due to the larger distance between the tip and the cantilever, the resolution of non-contact images is less than for contact images.

3.1.2.3 Tapping mode

This mode provides high-resolution topographic images and overcomes the problems associated with frictional forces, which might easily damage soft sample surface in contact mode. In this mode the tip is oscillated close to the surface and intermittently contacts the sample once in each oscillation cycle. Inelastic sample deformation is therefore avoided. The cantilever is oscillated with an amplitude of around 20nm. As the oscillating tip approaches the surface the cantilever amplitude is damped and the resonance frequency shifted to lower values. This decrease in oscillation amplitude is used to image topographical surface features. The main advantages of tapping mode are for example, that it prevents the tip from sticking and the avoidance of surface damage. The adhesive forces are reduced since a high frequency oscillation with high amplitude is used for the measurements. There are no shear forces acting on the sample surface. Tapping mode is therefore suitable for most routine sample measurements [5].

3.1.3 Atomic resolution and noise artifacts

There are many factors which affect the image resolution and generate artifacts. Those include the probe geometry and noise from the surroundings.

3.1.3.1 Probe geometry

Images acquired with an atomic force microscope represent both the probe geometry and the shape of the features being imaged [11-13]. If the probe is smaller than the features of interest, outline of these structures will be accurate and artifacts will be at a minimum. Blunt tips or probes with a large opening angle will cause steps to appear sloped and peaks to appear round. To obtain molecular resolution a very sharp probe with a high aspect ratio (length/width) is necessary and the instrument is operated at low forces of about 10^{-10} N [14], in order to minimize the contact area. Probes with high aspect ratio, are preferred for rough surfaces. In some cases, however, it is still possible to get accurate information from the image even if the probe is not as sharp as the object being imaged [15].

3.1.3.2 Thermal noise

One of the most significant sources of noise in an AFM image is thermal noise [16-18]. Drift in the images can occur because of thermal drift in the piezoelectric scanners and because the cantilever is susceptible to external temperature changes. Drift will cause lines that should appear straight to have a curvature. To minimize the effect of the thermal drift on geometrical parameters of the image, it is necessary to carry out the imaging after thermal equilibrium has been reached between the sample and microscope stage, i.e. leave the instrument on for a few hours before imaging and then conduct the measurements with high scanning speed [5].

3.1.3.3 Mechanical noise

Environmental vibrations produced by people moving in the building, elevators, street traffic or a person's voice are noticeable in the image [19]. This can cause the probe in the microscope to vibrate and make artifacts in an image. Typically, these appear as localized oscillations in the image. These artifacts can be reduced using an air table, that keeps the AFM level at all times.

3.1.3.4 Electronic noise

Image artifacts can become visible in AFM scans because of faulty or inadequate electronic components. This form of noise is as unavoidably present as the Brownian motion of the observed object and of the probe that is interacting with the objects at room temperature. Electronic artifacts most often appear as oscillations or repeating patterns in an image. Periodic artefacts can be removed by Fourier transformation, and filtering of the image, resulting in a clearer image [19].

3.2 Wide angle x-ray diffraction (WAXD)

Wide angle x-ray diffraction (WAXD) is a technique, which is frequently used to determine the crystal structure and the degree of the crystallinity of materials including polymers. This technique can be used to obtain qualitative and quantitative information of the crystal phases present in isotactic polypropylene.

3.2.1 Bragg's law

A monochromatic x-ray beam with the wavelength λ is scattered by the crystalline material at a specific angle θ . Due to the presence of regular (crystal) planes in the material, separated by the distance d as shown in Figure 3.3 [20, 21], two beams have a different path-length of $AB + BC = 2AB$. If $2AB$ is a multiple n of the wavelength λ , the two beams interfere constructive by. $2AB = n\lambda$ and with $AB/d = \sin\theta$ follows the Bragg equation: $2d \sin\theta = n\lambda$

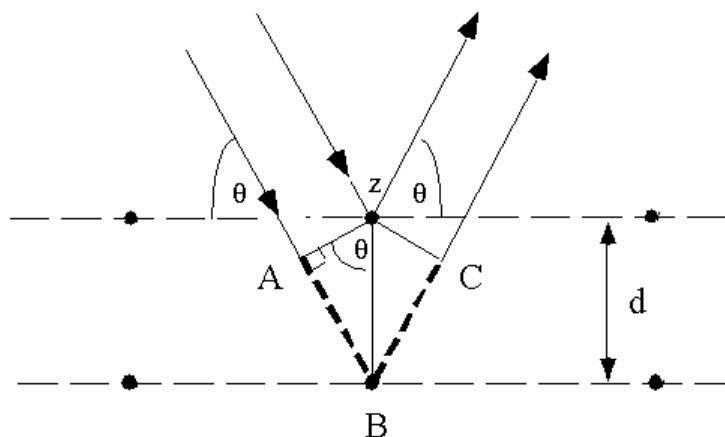


Figure 3. 3: An illustration of the diffraction conditions leading to Bragg's law [22].

3.2.2 Crystal lattice and indices

The unit cell is described by the axes a , b , c , as shown in Figure 3.4 and the angles between them are α , β , and γ . The values of the angles depend on the type of the unit cell. Across several unit cells, repeating crystallographic planes are present, which are indexed with hkl indices (Miller indices). The Miller indices indicate how the crystal

planes intersect the main crystallographic axes of the solid. A set of Miller (hkl) indices quantifies the intercept and can therefore be used to uniquely identify the plane. Figure 3.4 shows the example of a (110) plane [20].

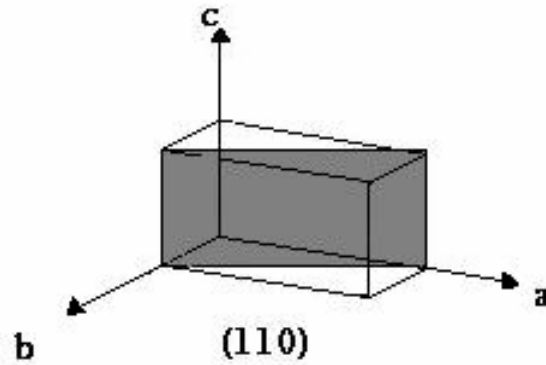


Figure 3. 4: A schematic illustration of the unit cell and the (110) plane [20].

In WAXD experiments the sample is exposed to monochrome radiation, typically originating from Cu-K α with a wavelength of $\lambda = 0.15418\text{nm}$, and the scattering angle θ is varied. If $\sin\theta$ equals $n\lambda/2d$ the beams interfere constructively and the spectrum shows a peak indicating that d equals the distance of two crystallographic planes. The spectra are mostly represented as a function of “ 2θ ”, which is the angle between the incoming and the reflected beam.

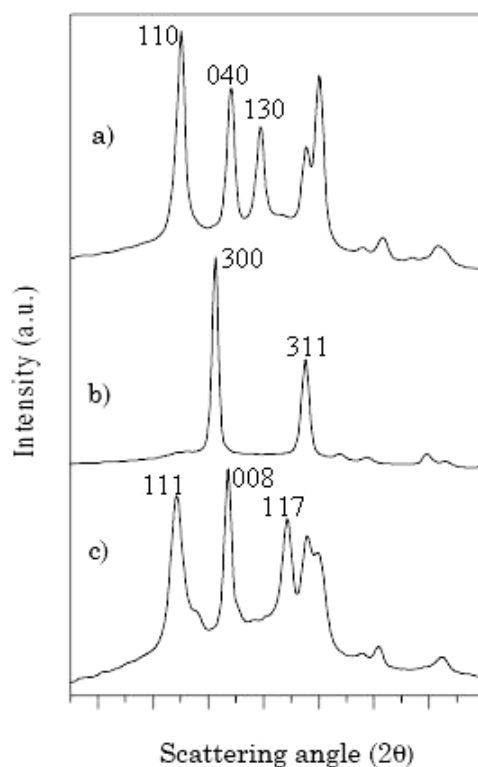


Figure 3. 5: A typical X-ray diffraction pattern of pure, a) α -, b) β - and c) γ -phase of iPP [23].

The different crystalline phases of iPP can be identified from the X-ray diffraction pattern, as shown in Figure 3.5. The peaks at $2\theta = 14.8^\circ$, 16.95° and 18.5° , which are related to the indices 110, 040 and 130 respectively, are typical for the α -phase. The 300 peak at $2\theta = 16.6^\circ$ is evidence for the presence of the β -phase. The 117 peak at $2\theta = 20.07^\circ$ is related to the γ -phase [22-24].

3.2.3 Determination of the degree of crystallinity

Semi-crystalline polymers consist usually of two phases, a uniform crystalline phase and an amorphous phase. In an x-ray diffraction curve of an unoriented sample, over a range of angles the crystalline diffraction peaks and the major portion of the amorphous halo can be separated. The mass crystallinity (ω_m) can be estimated by integrating over the area of the crystalline peaks (I_c) and dividing them by the total scattering (I_{tot}), which is the sum of both crystalline and amorphous (I_a) scattering [25].

$$\omega_m = \frac{I_c}{I_{tot}} = \frac{I_c}{I_c + KI_a} \quad \text{Eq. 3.1}$$

Where K is a calibration factor and assumed to equal to unity.

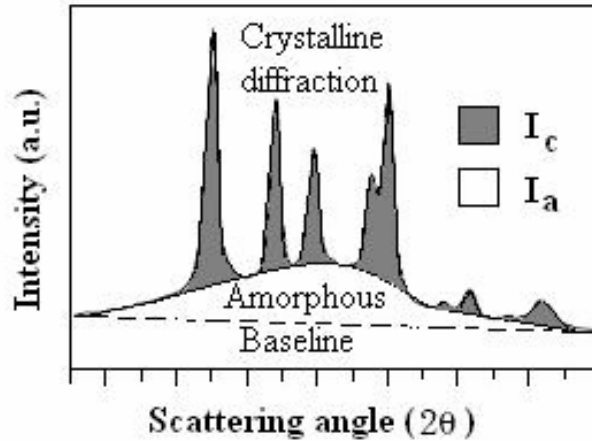


Figure 3. 6: Scattering curve for isotactic polypropylene showing the crystalline peaks and the amorphous background scattering [20].

3.2.4 Determination of the γ -phase content

The γ -phase content in the samples can be calculated from the X-ray diffraction pattern by determining the ratio between the peak intensities of the reflection (117) at $2\theta = 20.18^\circ$ and the reflection (130) at 18.68° , which are distinctive for the γ - and α -phase respectively. The intensities of the (117) and (130) reflections were measured from the area of the corresponding diffraction peaks above the diffuse halo in the X-ray powder diffraction pattern [26].

$$X_\gamma = \frac{I_{(117)\gamma}}{I_{(117)\gamma} + I_{(130)\alpha}} \quad \text{Eq. 3.2}$$

3.3 References

1. G. Binnig, H. Rohrer, C. Gerber, E. Weibel. *7 x 7 Reconstruction on Si (111) resolved in real space*. Physical Review Letters. 1983, **50**, 120-123.
2. L. Xu, X. W. Yao, L. P. Zhang, M. Q. Li, F.J. Yang. *Interpretations of atomic-resolution images in atomic-force microscopy*. Physical Review B. 1995, **51**, 10013-10017.
3. G. Binnig, C. F. Quate, Ch. Gerber. *Atomic force microscope*. Physical Review Letters. 1986, **56**, 930-933.
4. S. N. Magonov. *Atomic force microscopy in analysis of polymers*, in *Encyclopaedia of Analytical Chemistry*, R.A. Meyers, Editor. Wiley. 2000, 7433-7490.
5. W. Stocker, S. N. Magonov, H. J. Cantow, J. C. Wittmann, B. Lotz. *Contact faces of epitaxially crystallized α - and γ -phase isotactic polypropylene observed by atomic force microscopy*. Macromolecules. 1993, **26**, 5915-5923.
6. L. A. Bottomley, E. D. Gadsby, M. A. Poggi. *Microscopy techniques/Atomic Force and Scanning Tunnelling Microscopy*, in *Encyclopaedia of Analytical Science*, P. Worsfold, A. Townshwnd, C. Poole, Editors. Elsevier Academic Press. 2005, 397-408.
7. N. S. McIntyre H. Y. Nie. M. J. Walzak. *Atomic force microscopy study of biaxially-oriented polypropylene films*. International Surface Engineering Congress. 2003 293-302.
8. P. A. Maurice. *Applications of atomic-force microscopy in environmental colloid and surface chemistry*. Colloids and Surfaces. 1996, **107**, 57-75.
9. R. Erlandsson, P. Apell. *Progress in scanning probe microscopy: High resolution force microscopy and spectroscopy*. Current Science. 2000, **78**, 1445-1458.
10. M. Meincken, R. D. Sanderson. *Advantages of scanning probe microscopy in polymer science*. South African Journal of Science. 2004, **100**, 256-260.
11. W. A. Hofer, A. S. Foster, A. L. Shluger. *Theories of scanning probe microscopes at the atomic scale*. Reviews of Modern Physics. 2003, **75**, 1287-1332.
12. M. R. Jarvis, R. Pérez, M. C. Payne. *Can atomic force microscopy achieve atomic resolution in contact mode?* Physical Review Letters. 2001, **86**, 1287-

- 1291.
13. U. D. Schwarz, H. Holscher, R. Wiesendanger. *Atomic resolution in scanning force microscopy: Concepts, requirements, contrast mechanisms and image interpretation*. Physical Review B. 2000, **62**, 13089-13098.
 14. F. M. Ohnesorge. *Intricate steplike artifact can mimic true atomic resolution in atomic force microscopy*. Physical Review B. 2000, **61**, 5121-5125.
 15. S. S. Sheiko. *Imaging of polymers using scanning force microscopy: From superstructures to individual molecules*. Advances in Polymer Science. 2000, **151**, 61-174.
 16. F. J. Giessibl. *Advances in atomic force microscopy*. Reviews of Modern Physics. 2003, **75**, 949-984.
 17. S. M. Lindsay. *The scanning probe microscope in biology*, in *Scanning Probe Microscopy and Spectroscopy*, D. Bonnell, Editor. WILEY-VCH. 2000, 290-330.
 18. F. Gittes. C. F. Schmidt. *Thermal noise limitations on micromechanical experiments*. Eur Biophys J. 1998, **27**, 75-81.
 19. P. West, N. Starostina. *A Guide to AFM image artifacts*. Pacific Nanotechnology 2002 [cited 10/05/2005]; 1-12].
 20. C. Y. Li, B. Wang, S. Z. Cheng. *X-ray scattering in analysis of polymers*, in *Encyclopaedia of Analytical Chemistry*, R.A. Meyers, Editor. Wiley. 2000, 8105-8118.
 21. S. G-Granda, J. M. M-Bernardo. eds. *X-ray absorption and diffraction*. 2nd ed. Encyclopedia of Analytical Science, ed. P. Worsfold, A. Townshend, C. Poole. Vol. 9. Elsevier Academic Press. 2005, 397-408.
 22. S. V. Meille, S. Brückner. *X-ray Scattering*, in *Polypropylene An A-Z Reference*, J. Kargwr-Kocsis, Editor. Kluwer Academic Publishers. 1999, 890-895.
 23. S. Piccarolo T. Foresta, G. Goldbeck-Wood. *Competition between α and γ phases in isotactic polypropylene: effects of ethylene content and nucleating agents at different cooling rates*. Polymer. 2001, **42**, 1167-1176.
 24. R. Thomann, C. Wang, J. Kressler, R. Muelhaupt. *On the γ -phase of isotactic polypropylene*. Macromolecules. 1996, **29**, 8425-8434.
 25. J. H Chen, F. C Tsai, Y. H Nien, P. H Yeh. *Isothermal crystallization of*

isotactic polypropylene blended with low molecular weight atactic polypropylene. Part I. Thermal properties and morphology development. Polymer. 2005 **46**, 5680-5688.

26. R. Thomann, H. Semke, R. D. Maier, Y. Thomann, J. Scherble, R. Mulhaupt, J. Kressler. *Influence of stereoirregularities on the formation of the γ -phase in isotactic polypropene.* Polymer. 2001, **42** 4597-4603.

4 Experimental

4.1 Materials and sample preparation

4.1.1 Isotactic polypropylene

One sample of isotactic polypropylene has been investigated. It was provided by Sasol (South Africa). The molecular characteristics are not of major importance in the present study, since the crystallographic interactions at the unit-cell level were investigated.

The pellets of isotactic polypropylene were hot-pressed into a film at 190°C. This thin film of α -iPP was heated again to 190°C for 5 min to remove the thermal history of the material and then crystallized in an isothermal process at 130°C for 24h in vacuum to prevent degradation. Subsequently it was cooled down to room temperature at a cooling rate of 20°C/h.

4.1.2 Propylene-ethylene random copolymers

Samples (A and B) of polypropylene-ethylene random copolymers were obtained from [1]. Fractions were obtained from preparative temperature rising elution fractionation of these two commercial samples. Fractions PPE1 – PPE3 originate from sample A and Fractions PPE4 – PPE6 from sample B. The properties of the fractionated samples are presented in Table 4.1.

Table 4. 1: Characteristics of propylene-ethylene co-polymers.

Sample name	Fraction label	Molecular weight (Mw)	Mw/Mn	Ethylene content (mol %)
A	PPE1	248874	2.63	3.25
	PPE2	369246	3.21	1.75
	PPE3	288559	3.10	1.00
B	PPE4	199564	2.85	2.80
	PPE5	310260	2.60	2.25
	PPE6	172971	3.15	1.80

4.1.3 Propylene-ethylene block copolymers (impact polypropylene)

Samples of impact polypropylene with varying ethylene content were supplied as pellets from Sasol. The characteristics of these samples are presented in Table 4.2.

Table 4. 2: Characteristics of propylene-ethylene block copolymers.

Sample name	Molecular weight (Mw)	Mw/Mn	Ethylene content (mol %)
PEB1	266276	4.1	12.0
PEB2	234531	2.9	9.5
PEB3	368913	3.8	6.5

4.1.4 Propylene-pentene random copolymers

Samples of polypropylene-pentene random copolymers were provided by Sasol. The characteristics of these samples are presented in Table 4.3.

Table 4. 4: Characteristics of propylene-pentene random copolymers.

Sample symbol	Molecular weight	Mw/Mn	Pentene content (mol %)
PPe1	324800	3.59	2.29
PPe2	368400	4.95	1.18
PPe3	355500	4.43	1.75
PPe4	339200	4.36	0.92

Samples of the α - and γ -phase from propylene-ethylene random copolymers, polypropylene-ethylene block copolymers (impact polypropylene) and polypropylene-pentene copolymers were prepared as follows: the samples were hot-pressed at 230°C into 100 μ m thick films. These films were melted at 190°C under vacuum in an oil bath equipped with a temperature controller, and were slowly cooled to room temperature at a rate of 2°C/ h.

4.2 Permanganic etching of the iPP Sample

The permanganic reagent used was a 7% mass/volume solution of potassium permanganate in concentrated sulphuric acid, prepared by adding the permanganate slowly to the acid in a conical flask with rapid agitation. After the permanganate was added, the flask was shaken occasionally until all the crystals had dissolved. The samples were immersed in this solution for 1 hour. Subsequently the films were washed with methanol [2-4].

4.3 Set-up of the instrumentation

4.3.1 Wide angle x-ray diffraction (WAXD)

The mass crystallinity and the content of the α - and γ -phase were determined from WAXD data, obtained from samples that were isothermally crystallized and then cooled to room temperature. The analysis was performed at iThemba LABS/ South Africa on a Bruker AXS D8 ADVANCE diffractometer at room temperature with filtered $\text{CuK}\alpha$ radiation. All samples were scanned at 2θ angles ranging from 9° to 36° with a sampling width of 0.02° , where 2θ is the diffraction angle.

4.3.2 Atomic force microscope

All AFM measurements were performed with a Multimode AFM with a Nanoscope IIIa controller from Veeco in ambient conditions. The methods used to set-up and calibrate the AFM for imaging, were based on the procedures given in the instruction manual [5].

The AFM was operated in the contact mode. In this mode the tip deflection is kept constant by a feedback loop and differences in height are represented by differences in the voltage applied to the piezo in order to keep the distance between tip and sample constant. Before the polypropylene samples were imaged the instrument was calibrated.

4.3.2.1 AFM calibration

For calibration of the piezo scanner of the AFM, a freshly cleaved mica surface was imaged. The calibration was carried out as described in the manual [5] in ambient conditions. The scan size was $6 \times 6 \text{ nm}^2$, and the scan rate 61 Hz in order to defeat noise due to thermal drift. Images were acquired with the A-scanner and a V-shaped contact cantilever. The lateral distances measured after the calibration showed an inaccuracy of less than 2%.

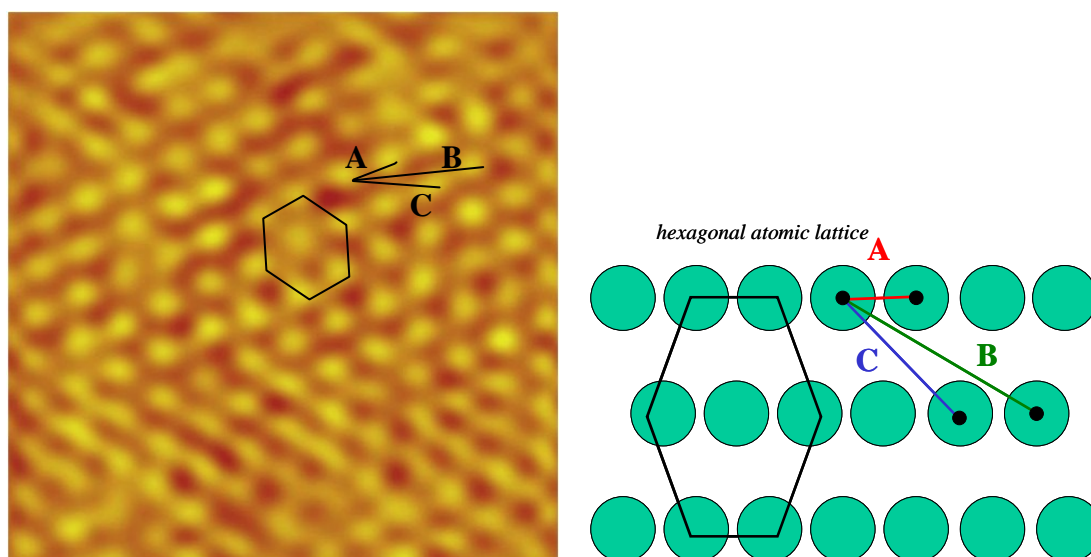


Figure 4. 1: a) Fourier-filtered AFM image of mica with a size of $6 \times 6 \text{ nm}^2$ indicating the measured distances $A=0.528 \text{ nm}$, $B=1.379 \text{ nm}$, $C=0.909 \text{ nm}$. b) The schematic drawing shows the expected distances of mica: $A=0.519 \text{ nm}$, $B=1.37 \text{ nm}$, $C=0.900 \text{ nm}$.

4.3.2.2 Sample imaging

The cantilevers used for low-resolution imaging on a μm -scale were silicon cantilevers with a spring constant of $0.07\text{-}0.4 \text{ N/m}$ while V-shaped silicon nitride cantilevers with the lowest possible spring constants were used for the high resolution images to cause as little damage as possible on the sample surface during scanning, and also to detect the small atomic forces between tip and sample. After the tip was placed in the tipholder, the position of the laser was focused on the free end of the cantilever with the help of an optical microscope attached to the AFM.

All samples were prepared as a film. These films were cut into pieces of $1 \times 1 \text{ cm}^2$ and stuck to the sample holder using double sided adhesive tape.

The best images were obtained by using the height mode with feedback gains as low as possible in order to obtain noise-free images without oscillations from the feedback system.

For μm -scale images the E (maximum scan size about $13 \mu\text{m}$) and JHV (maximum scan size about $130 \mu\text{m}$) scanners were used. The instrument setup was 512 data samples per scan line, a scan rate of $0.7\text{-}1.0 \text{ Hz}$, an integral gain of $4\text{-}6$, a proportional gain of approximately $6\text{-}8$ and a set point of 0 volt .

To minimize potential artifacts from tip broadening due to contamination, the tip was replaced with a new tip whenever the images were not reproducible any longer.

For the high resolution images (nano-scale imaging) the A scanner was used (maximum scan size about 1.3 μm). First a “large” 1.3x1.3 μm^2 image of the surface was obtained and the scan range then slowly zoomed in to smaller ranges, down to about 10x10 nm^2 . The scan angle, set point, feedback gains, and scan rate were optimized to obtain the clearest possible images without artifacts. The optimal settings were: 512 data samples per scan line, a scan rate of 61 Hz, an integral gain of 4-6, a proportional gain of approximately 13-20 and a set point of 0 Volt.

All images were enhanced in the imaging program and subjected to a plane fitting and flattening procedure, which eliminates the image bow resulting from non-linear scanner movement.

For atomic resolution images additional digital filtering was carried out to remove noise and clarify the periodic structures present in the image. Since the filtering is a very sensitive process that can generate unreal features or remove existing features, the filtering was kept to a minimum. Only noise and image artifacts were eliminated.

The typical sequence of digital filtering applied was: auto-flattening, planefit, lowpass filtering, and 2-dimensional fast-Fourier transformation (2D-FFT).

- Auto flattening eliminates the image bow by calculating a least square fitted, second order polynomial for each scan line and subtracting it from the scan line.

- The planefit removes the effect of a skew sample by calculating a best, second order polynomial planefit and subtracting it from the image. It can be applied to both the x and y direction.

- Lowpass filtering is used to remove high frequency noise, such as spikes by replacing each data point in the image with a weighted average of the points in a 3x3 matrix surrounding the point.

- A 2D-FFT is used to select the periodic information from the image and suppress noise. Fourier filtering is a powerful technique which, if judiciously and carefully

used, can improve images greatly. Incorrect Fourier filtering of an image can alter the observed surface structure by selective removal of spots at reciprocal lattice sites in the Fourier transformed image. Figure 4.2b shows an example of the Fourier transformation of the image in Figure 4.2a. The periodic structure indicated by boxes in Figure 4.2c is surrounded by noise before filtering. The points form a hexagonal pattern, which provides further evidence for the hexagonal structure of mica. Figure 4.2c is the Fourier transformed image before filtering and Figure 4.2d, shows the Fourier transformed images of the surface after the Fourier transformation.

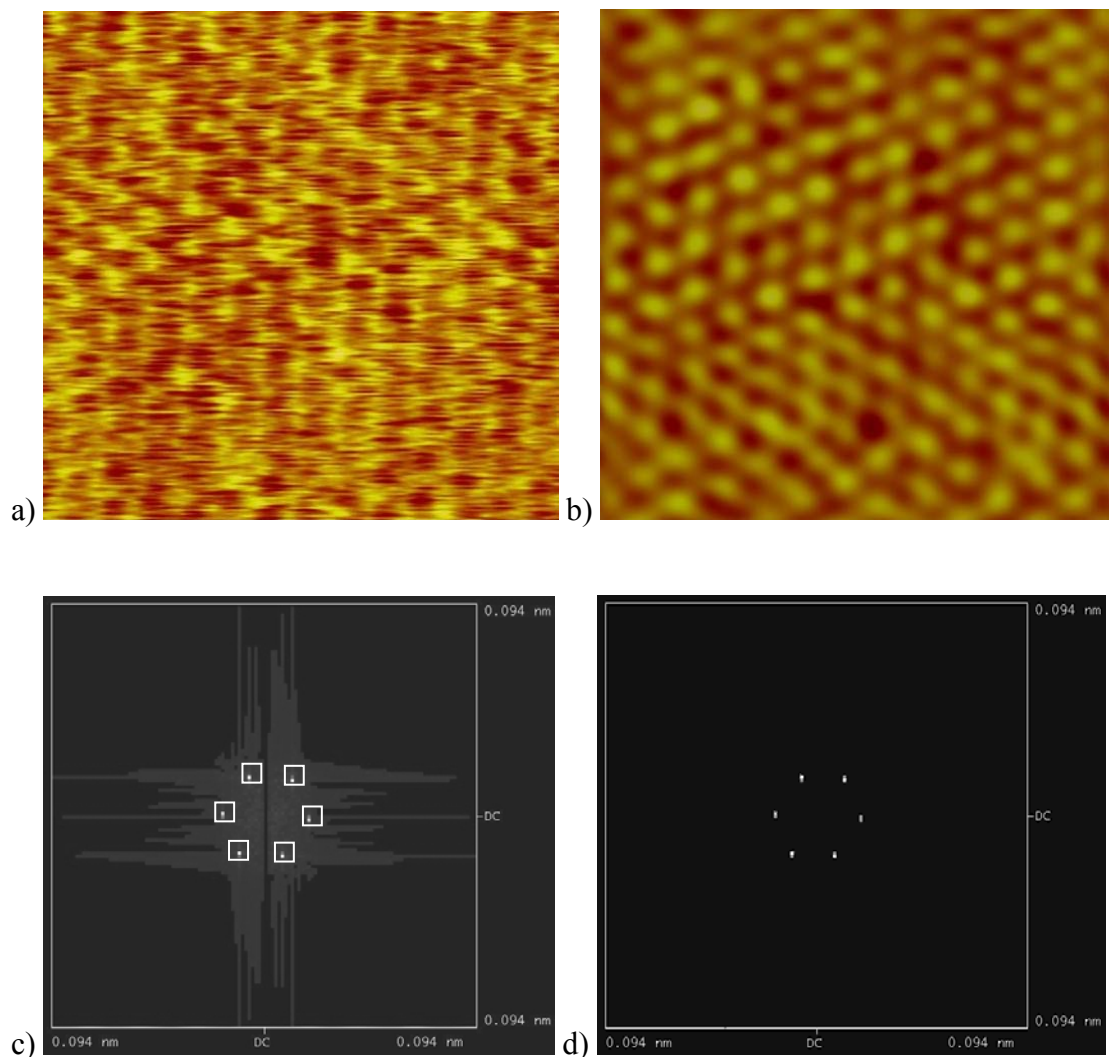


Figure 4. 2: a) AFM image of mica before filtering and b) AFM image of mica after filtering, c) Fourier transformed image of mica before filtering, d) Fourier transformed image after filtering.

After the image is processed, it is analysed and characteristic surface structures, such as the distance, periodicity, angle, etc. can be determined.

Acquiring AFM images at molecular resolution is not easy and typically needs hours or days of operation and adjustment of the control values and settings of the instrument for one sample.

There are many factors responsible for the difficulty in obtaining AFM images at high resolution. One of most important factors is the AFM's sensitivity towards noise from the surroundings. The instrument must be carefully isolated from electrical and mechanical noise and vibrations. The latter can typically be minimized by using an air table. Electrical noise from other machines may also affect the instrument. The best resolution (a higher signal to noise ratio) is often obtained at night or during weekends to avoid noise from the surroundings. Blunt tips can also reduce the resolution. Loading the tip into the tip-holder is difficult and a small error in handling might damage the tip. Besides this, the surface must be flat, otherwise the tip engagement might be a problem and the z-piezo range could be exceeded while scanning. Surface contaminants can often obstruct images of structures at molecular resolution.

4.4 Difficulties

The main problem with the iPP samples, however, is the orientation of the crystal planes of interest, which are mostly perpendicular to the surface and can therefore not be imaged by AFM. Although the preferred growth direction of the dominant radial lamellae has been determined to be the a direction, with the chain axis (c-axis) nearly normal to the radial direction, the two possible contact faces of the a-c (010) plane are frequently not accessible for AFM direct visualization for several reasons. Firstly, iPP is a semi-crystalline polymer, which consists of both amorphous and crystalline regions and it can never reach a 100% crystallinity. Secondly, the spherulites usually grow in three dimensions, which results in the fact that the a-c plane is hidden inside the spherulite, unless a very thin film is made. Since the AFM can only image the topmost surface layer it will in most cases not be possible to image the crystalline a-c plane and the ordered methyl groups. The crystalline area can only be imaged if lamellae twisting occurred during the crystallization so that the a-c plane points to the surface.

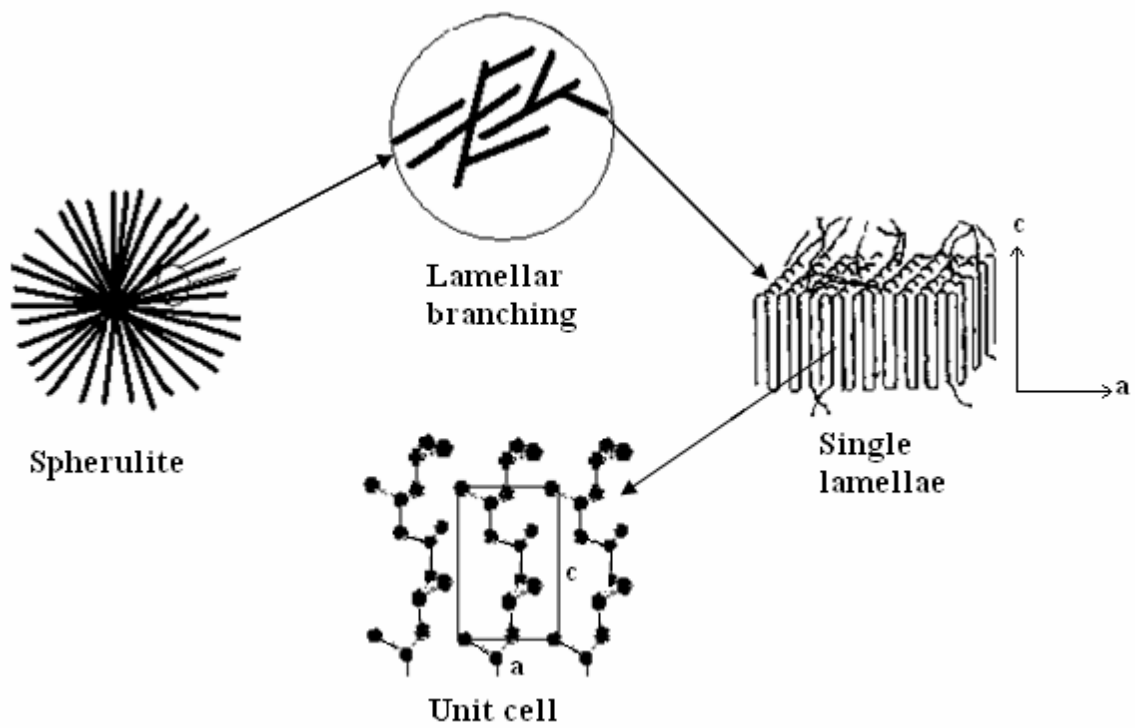


Figure 4. 3: Schematic illustration of the building blocks of iPP crystals.

4.5 References

1. G. Harding. *The fractionation and characterisation of commercial polypropylene random copolymers*. Dep. Chemistry and Polymer Science. University of Stellenbosch. 2005
2. I. L. Hosier, R. G. Alamo, J. S. Lin. *Lamellar morphology of random metallocene propylene copolymers studied by atomic force microscopy*. Polymer. 2004, **45**, 3441–3455.
3. R. H. Olley, D. C. Bassett. *On the development of polypropylene spherulites*. Polymer. 1989, **30**, 399-409.
4. R. Thomann, H. Semke, R. D. Maier, Y. Thomann, J. Scherble, R. Mulhaupt, J. Kressler. *Influence of stereoirregularities on the formation of the γ -phase in isotactic polypropene*. Polymer. 2001, **42** 4597-4603.
5. Digital Instruments Veeco Metrology Group. *MultiModeTM SPM Instruction Manual Version 4.31ce*. 1996.

5 Results and Discussion

5.1 Wide-angle X-ray diffraction

Wide-angle X-ray diffraction is used mainly in the structural characterization of atomic or molecular periodicity in crystalline materials. This technique was used on the samples in order to determine the percentage of crystallinity and the content of the γ -phase to be used for comparison with the AFM results.

The mass crystallinity (ω_m) was estimated by integrating over the crystalline peaks (I_c) and dividing them by the total scattering (I_{tot}), which is the sum of both crystalline and amorphous (I_a) scattering, as described in Section 3.2.3, Equation (3.1).

The different crystalline phases of iPP could be identified from the X-ray diffraction. The peaks at $2\theta = 14.8^\circ$, 16.95° and 18.5° relate to the indices 110, 040 and 130 respectively and are typical for the α -phase. The 117 peak at $2\theta = 20.07^\circ$ is related to the γ -phase.

The γ -phase content in the samples was calculated from the X-ray diffraction pattern, by determining the ratio between the peak intensities of the reflection (117) at $2\theta = 20.18^\circ$ and the reflection (130) at 18.68° , which are distinctive for the γ - and α -phase respectively. The intensities of the (117) and (130) reflections were measured from the area under the corresponding diffraction peaks above the diffuse halo in the X-ray powder diffraction pattern, as described in section 3.2.4, equation (3.2). The degree of crystallinity and the α - and γ -phase content are presented in Tables 5.1-5.4.

5.1.1 Isotactic polypropylene

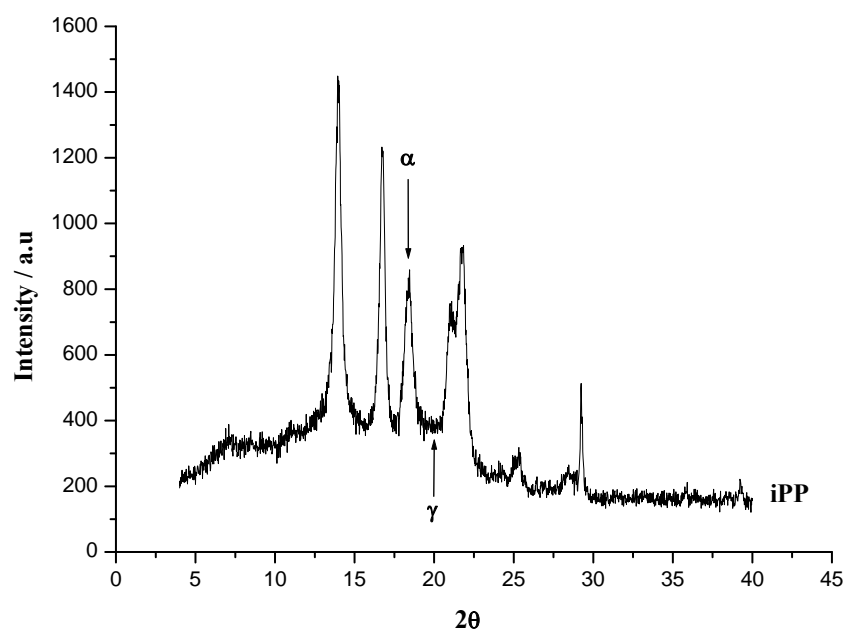


Figure 5. 1: WAXD pattern of iPP melt crystallized at 130°C.

The WAXD pattern of iPP melt crystallized at 130°C is displayed in Figure 5.1 It shows a typical pattern of the α -phase, confirmed by the presence of the reflection (130) at $2\theta = 18.68^\circ$ and the absence of the reflection (117) at $2\theta = 20.18^\circ$, which is characteristic for the γ -phase.

It has been reported that iPP samples prepared with a commercial, heterogeneous Ziegler-Natta catalyst, crystallize mainly in the α -phase [1]. This can be attributed to the uneven distribution of defects along the polymer chains. The distribution of tacticity in the Ziegler-Natta derived samples is not homogeneous over the molecular weight distribution and also not homogeneous within the chains itself. Ziegler-Natta samples have a blocky distribution of the stereo-defects. The defects are accumulated in a small portion of non-crystallizable chains or form small blocks of irregular sequences among long regular chains. This leads to long regular isotactic sequences, which favour the formation of the α -phase.

Table 5. 1: Isotactic polypropylene with its degree of crystallinity and the percentage of different crystal phases.

Sample name	Degree of crystallinity (%)	Ethylene content (%)	α -phase crystal content (%)	γ -phase crystal content (%)
iPP	57.20	0.0	100	0.0

5.1.2 Propylene-ethylene random copolymers

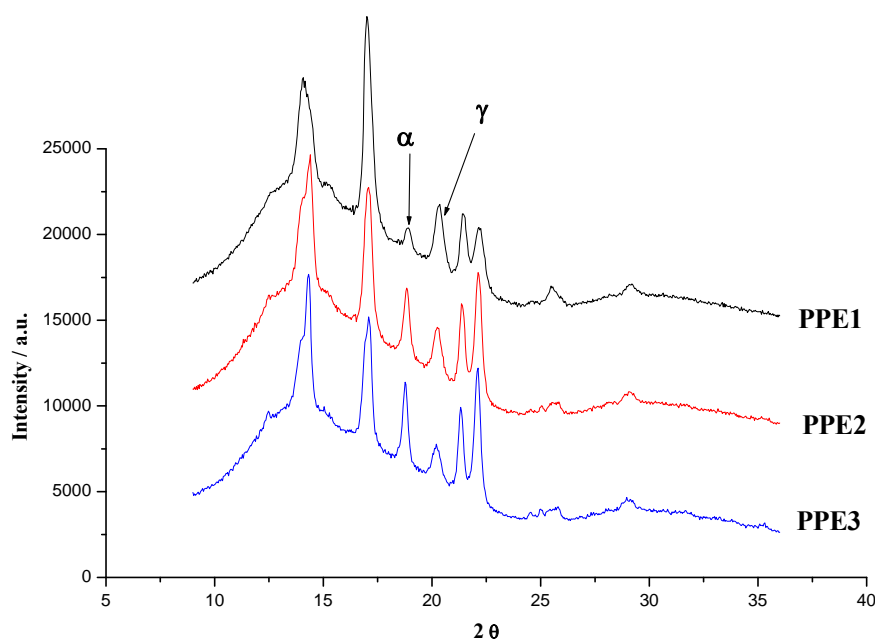


Figure 5. 2: WAXD pattern of PPE samples melt-crystallized at a slow cooling rate of 2°C/ h.

WAXD patterns of melt-crystallized PPE1, PPE2 and PPE3 with an ethylene content of 3.25, 1.75 and 1.00% respectively are presented in Figure 5.2. The distinctive reflections of both the α -phase and the γ -phase can be observed. This indicates that a blend of both the α - and γ -phase is found in the samples. Figure 5.2 also shows that the γ -phase content (the peak intensities of the reflection (117) at $2\theta = 20.18^\circ$) decreases as the ethylene content decreases in the sample. The same results were obtained for PPE4-PPE6, which are summarized in Table 5.2. This agrees with results obtained by Alamo et al.[1].

It has been reported that the formation of the γ -phase is favoured in the presence of stereo-defects and regio-defects, and also by the presence of comonomer units, which shorten the regular isotactic sequences [2]. The γ -phase also increases with decreasing cooling rate or increasing the crystallization temperature. The final amount of α - and γ -phase depends on both the comonomer content and crystallization temperature.

The structure of propylene-ethylene random copolymers is analogous to isotactic polypropylene, but the ethylene units, which are introduced randomly along the polypropylene chain, disrupt the regular repeating structure. This effect is similar to that of increasing atacticity and increases the mobility of the polymer chain as a result of less steric hinderance of the pendant methyl groups of polypropylene. It also reduces the crystallinity compared to isotactic polypropylene. This comonomer unit can be either included into the crystal structure or excluded from the crystalline areas into the amorphous phase.

Table 5. 2: propylene-ethylene co-polymer samples with their degree of crystallinity and the percentage of different crystal phases.

Sample name	Fraction label	Degree of crystallinity (%)	Ethylene content (%)	α-phase crystal content (%)	γ-phase crystal content (%)
A	PPE1	52.78	3.25	26.18	73.92
	PPE2	64.40	1.75	58.36	41.64
	PPE3	58.28	1.00	70.33	29.67
B	PPE4	57.80	2.80	34.02	65.98
	PPE5	63.30	2.25	87.77	12.33
	PPE6	58.95	1.80	87.93	12.07

5.1.3 Propylene-ethylene block copolymers

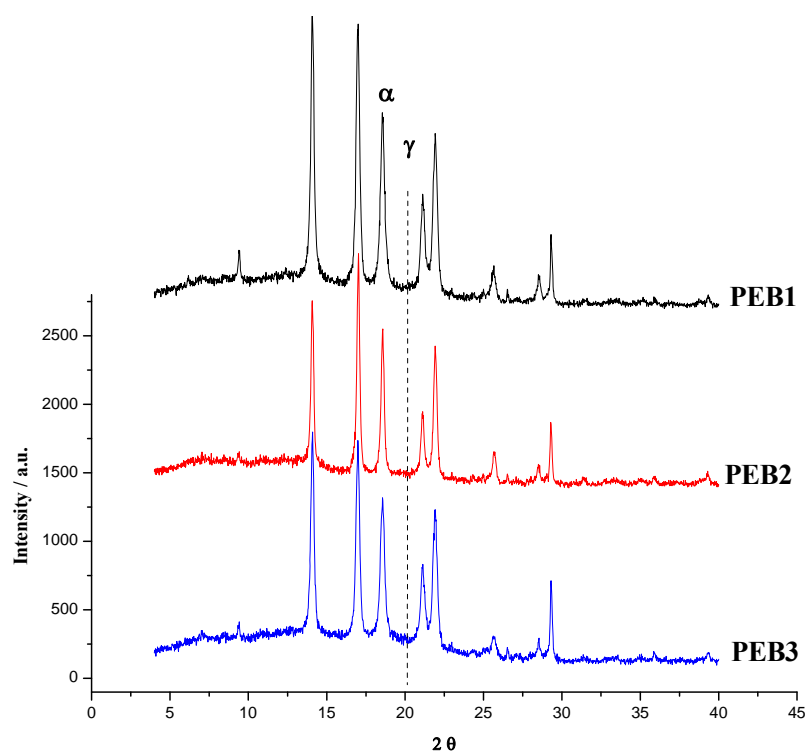


Figure 5. 3: WAXD pattern of PEB samples melt-crystallized at a slow cooling rate of $2^\circ\text{C}/\text{h}$.

WAXD patterns of melt-crystallized PE1, PEB2 and PEB3 with an ethylene content of 12.0, 9.5 and 6.5% respectively are presented in Figure 5.3. They show the typical pattern of the α -phase similar to that obtained for iPP, as indicated by the presence of the reflection (130) at $2\theta = 18.68^\circ$ and the absence of the reflection (117) at $2\theta = 20.18^\circ$, which is characteristic for the γ -Phase. Figure 5.3 shows that the presence and the variation of the ethylene content as a comonomer did not encourage the formation of the γ -phase. This can be explained by the fact that impact copolymers containing ethylene-propylene rubber are made in a two-stage process. The homopolymer produced in the first reactor is transferred to a second reactor, where the copolymerization with ethylene is carried out to produce ethylene-propylene rubber within the polypropylene matrix. This results in a product with the copolymer sequence ranging from polypropylene-like to polyethylene-like molecules, which leads to very long regular isotactic sequences, which usually crystallize only in the α -phase. The ethylene sequences do not crystallize with propylene but form an ethylene rich rubber phase incorporated in the polypropylene matrix.

Table 5. 3: Propylene-ethylene block copolymer samples with their degree of crystallinity and the percentage of different crystal phases.

Sample name	Degree of crystallinity (%)	Ethylene content (%)	α -phase crystal content (%)	γ -phase crystal content (%)
PEB1	64	12.0	100	0.0
PEB2	69	9.5	100	0.0
PEB3	65	6.5	100	0.0

5.1.4 Propylene-pentene random copolymers

WAXD results of melt-crystallized PPe1, PPe2, PPe3 and PPe3 with various pentene contents are presented in Table 5.4. It shows that the random incorporation of the 1-pentene comonomers promotes the formation of γ -phase, and the γ -phase content increases as the pentene contents increase. The effect of the 1-pentene is similar to that of the ethylene comonomer in a polypropylene-ethylene random copolymer. The presence of the 1-pentene comonomer units shortens the regular isotactic sequences, which favours the formation of the γ -phase.

Table 5. 4: Propylene-pentene random copolymer samples with their degree of crystallinity and the percentage of different crystal phases.

Sample symbol	Degree of crystallinity (%)	Pentene content (%)	α -phase crystal content (%)	γ -phase crystal content (%)
PPe1	52.68	2.29	47.82	52.18
PPe2	56.36	1.18	52.94	47.06
PPe3	55.50	1.75	58.72	41.28
PPe4	60.91	0.92	77.14	22.86

5.2 Atomic force microscopy

The morphology features of isotactic polypropylene and polypropylene copolymers of melt crystallized thin films have been studied. The thin films were prepared as described in section 4.1 and were analyzed by AFM.

5.2.1 Isotactic polypropylene

Isotactic polypropylene, which crystallized from the melt at 130°C, did not show the expected clear spherulite structure on a μm -scale. This can be explained by the formation of an amorphous layer on the surface. This amorphous layer consists of uncrystallisable material, which migrates to the surface during the crystallization process. It consists mainly of short chains with a high percentage of defects.

For nm-scale measurements without etching both the regular structure of the α -phase and complete amorphous regions could be observed, as illustrated in Figure 5.4.

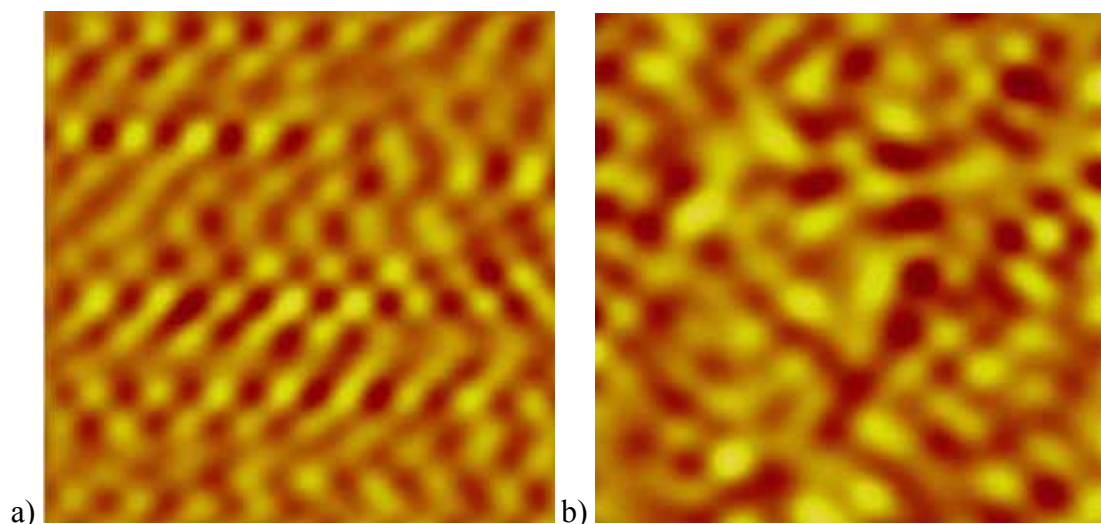


Figure 5. 4: $3 \times 3 \text{ nm}^2$ AFM height images of iPP a) crystalline α -phase, b) amorphous region of the same sample.

Figure 5.4 shows AFM height images of iPP where 5.4a represents a regular structure, which can be identified as α -phase due to the fact that the β angle is about 82° and the average dimensions of the unit cell are $a = 6.04 \text{ \AA}$ and $c = 5.94 \text{ \AA}$, showing an error of

9.17 % and 8.61% respectively compared to the typical α -phase unit cell dimensions [3, 4]. This error might be related to imperfections in the crystal structure of the polymer, as well as the experimental conditions such as a high scan rate of 61 Hz and large a tip diameter. These results confirm, however the high presence ($\sim 100\%$) of the α -phase obtained by X-ray results. On the other hand amorphous regions were detected on the same sample, as shown 5.4b.

5.2.2 Propylene-ethylene random copolymers

In contrast to isotactic polypropylene sample the propylene-ethylene random copolymers showed both α - and γ -spherulites on micro-scale and nano-scale without etching of the surface. This could be due to the fact that the samples were obtained from preparative temperature rising elution fractionation, which led to the removal of a big portion of un-crystallisable material (short chains with a high percentage of defects) from the samples.

5.2.2.1 The α -phase

The Figures 5.5-5.8 show the morphology of propylene-ethylene random copolymers containing a high percentage of the α -phase with different scales.

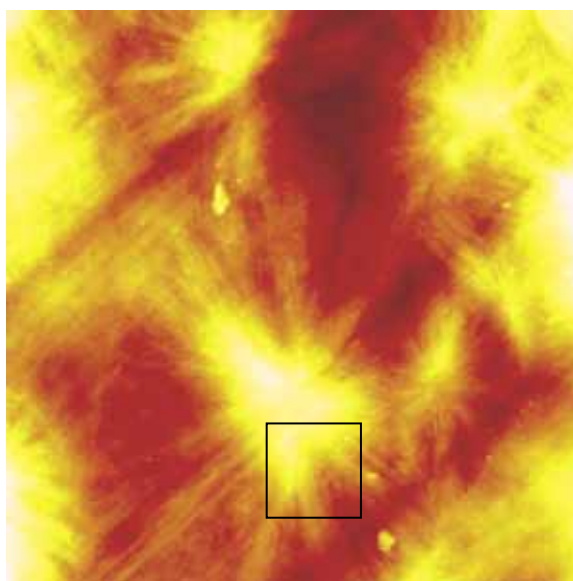


Figure 5. 5: 50x50 μm^2 AFM height image of PPE5 with 87.77% α -phase.

Figure 5.5 shows typical α -spherulites with diameters ranging from 10 to 30 μm obtained from the melt crystallized sample PPE5 with 87.77% α -iPP. The dark colours represent lower regions than the light colours. In this image the lamellae can be observed in the radial direction, which indicates that the lamellae grew from the centre outwards. This is observed more clearly in Figure 5.6. The micrograph does however not distinguish between the different types of α_{I} or α_{II} spherulites, or a mixture of both (see section 2.2.1.3), as they were reported by Padden and Keith [5] and later explained by Norton and Keller [6].

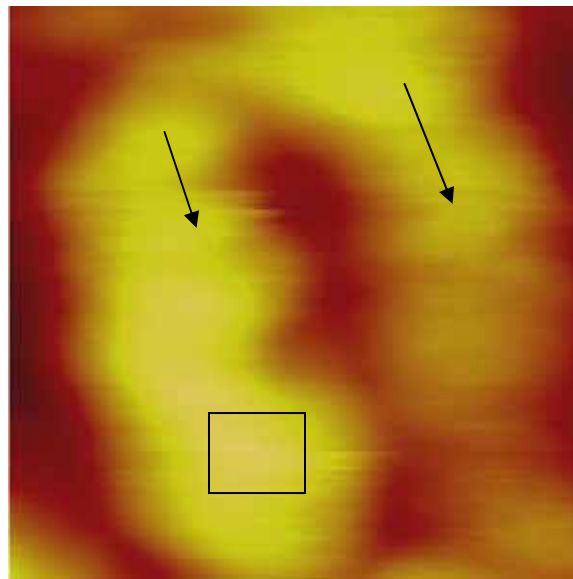


Figure 5. 6: 220x220 nm² AFM image, magnified from Figure 5.5.

Figure 5.6 shows the lamellar structure with an average lamellae thickness of 65 nm. It was acquired in the centre of Figure 5.5. The arrows indicate the radial direction of the lamellae. The box indicates the area, in which the images with high resolution (Figure 5.7) were acquired.

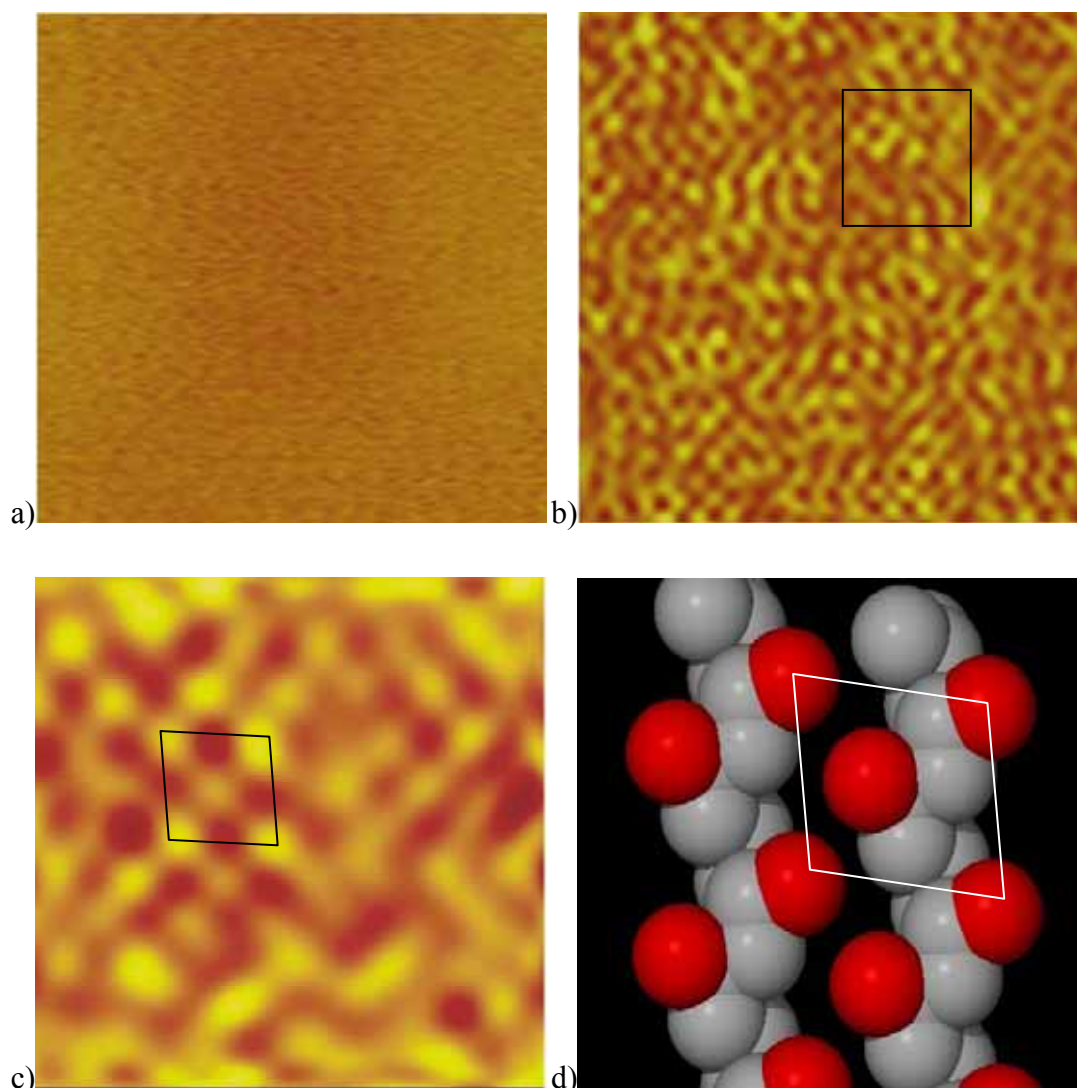


Figure 5. 7: a) Unfiltered AFM image of PPE5, scan size $11 \times 11 \text{ nm}^2$, b) Fourier-filtered version of a), c) a section of b) of $3 \times 3 \text{ nm}^2$, d) model produced with X-seed to illustrate the ac plane of a α -phase crystal structure (Five pattern) [7].

Figure 5.7a shows an unfiltered AFM image with a scan size of $11 \times 11 \text{ nm}^2$, which was acquired on the lamellar structure in Figure 5.6. Although the image is not very clear, because of electronic noise, it still shows some structures arranged in a regular pattern. Figure 5.7b shows the Fourier transformed image of Figure 5.7a, which clearly reveals the methyl groups of the polypropylene chains. It can be seen, that the methyl groups are arranged in a lozenge-shaped pattern and that the chain direction is almost normal to the lamellar surface in Figure 5.6, which is in good agreement with results reported by Stocker et al. [8]. Figure 5.7c shows a higher resolution image with a scan size of $3 \times 3 \text{ nm}^2$ enlarged from Figure 5.7b. The methyl groups on the a-c (010) plane show a distinctive five pattern (like the 5 on a dice). The five-face pattern

occurs when two methyl groups are exposed along the $\pm b$ axis direction, which is common for the α -phase of the crystal structure. The angles of this lozenge are 101° and 79° , which corresponds well to the values reported in literature [3, 8]. The measured dimensions of the unit cell are $a = 5.98 \text{ \AA}$ and $c = 6.12 \text{ \AA}$ with an error of 9.98% and 5.82%, respectively. Figure 5.7d shows a model produced with X-seed to illustrate the a-c plane of the α -phase crystal structure revealing the five pattern on the surface.

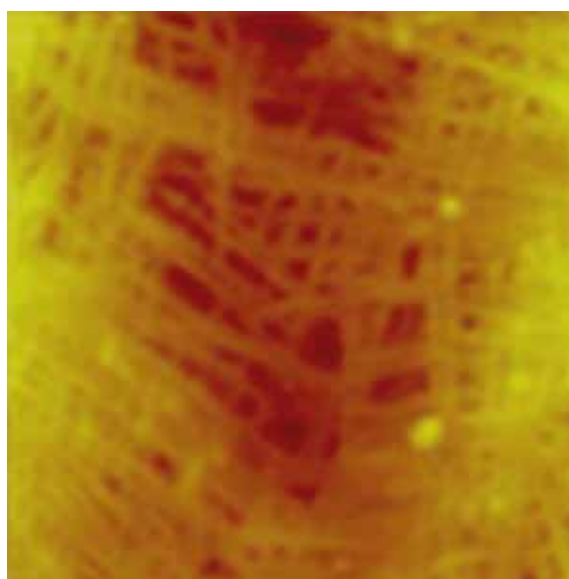


Figure 5. 8: $3 \times 3 \mu\text{m}^2$ AFM micrograph displaying cross-hatching of the PPE2 sample.

The morphology of the copolymer, sample PPE2 containing $\sim 1.75 \text{ mol \%}$ ethylene is shown in Figure 5.8. Similar results were also observed for PPE1 with 3.25 mol \% ethylene. It clearly shows the cross-hatching phenomenon of iPP. Some branching is observed with an angle of 80° , which is characteristic for α - α branching. This morphology feature is illustrated schematically in Figure 2.5. The cross-hatching phenomenon has been observed for both solution-crystallized and melt crystallized α -iPP. The preferred growth direction of the dominant radial lamellae has been determined to be the a direction, with the chain axis (c-axis) nearly normal to the radial direction. It has been proposed that the 80° or 100° branching angle corresponds to the matching of the a- and c-axis pair in the radial lamellae with the c- and a-axis of the tangential lamellae [4, 9]. This is due to the approximately identical a- and c-axis unit cell parameters 6.65 \AA and 6.5 \AA respectively. It has also been

proposed that branching occurs whenever two successive a-c layers are made of the same hand, for example, LRLRRLR or LRLRL, whereas the crystallographic unit cell consists of layers of opposite orientation [10]. The image also shows some of the branching with a branching angle of 40° . This later branching is characteristic for the epitaxial nucleation of the γ -phase crystals on the α -phase.

5.2.2.2 The γ -phase

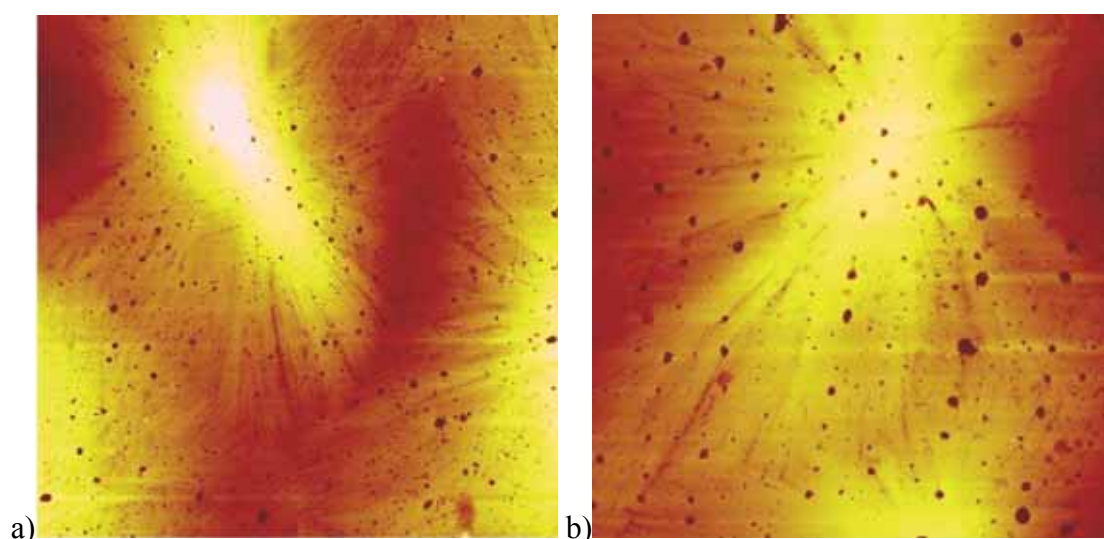


Figure 5. 9: AFM images of PPE1 with 73.92% γ -phase with a scan size of a) $100 \times 100 \mu\text{m}^2$, b) $60 \times 60 \mu\text{m}^2$.

Figure 5.9 shows the spherulite morphology of the γ -phase, which is different from the spherulites formed by the α -phase. The γ -spherulite in this image consisting of lamellae in a feather-like structure with angles of 40° or 140° between the lamellae. This type of morphology was confirmed for the first time by Khaled and Phillips [11] using SEM and AFM in tapping mode on etched iPP samples melt crystallised at high pressure of 200 MPa. The form of the lamellae was explained by two models: either by an epitaxial crystallization of γ -lamellae with a 40° angle to the radial α -lamellae, or by branching of the γ -lamellae at an angle of 140° on the surface of another γ -lamella, as it can be seen from the schematic illustration in Figure 5.10a and 5.10b.

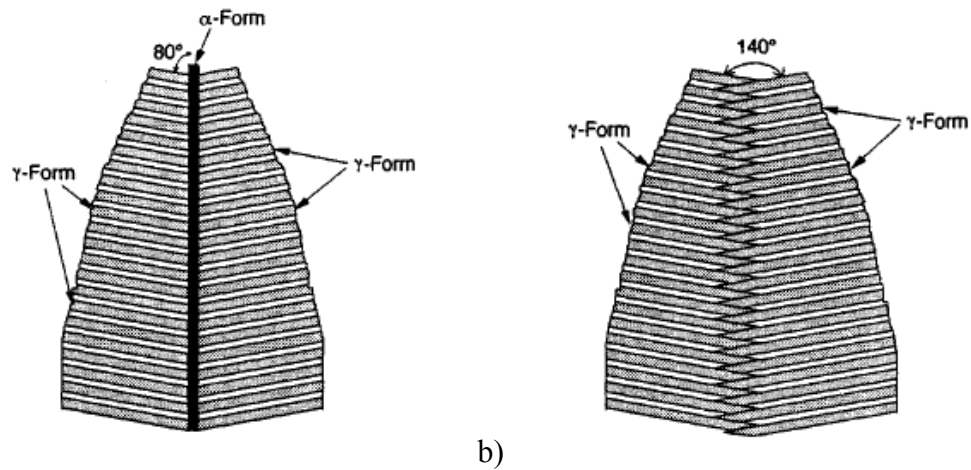


Figure 5. 10: Scheme of the growth mechanism of the feather-like structure of γ lamellae. a) Epitaxial growth of γ -lamellae on α -lamellae. b) Epitaxial growth of γ -lamellae on γ -lamellae [11].

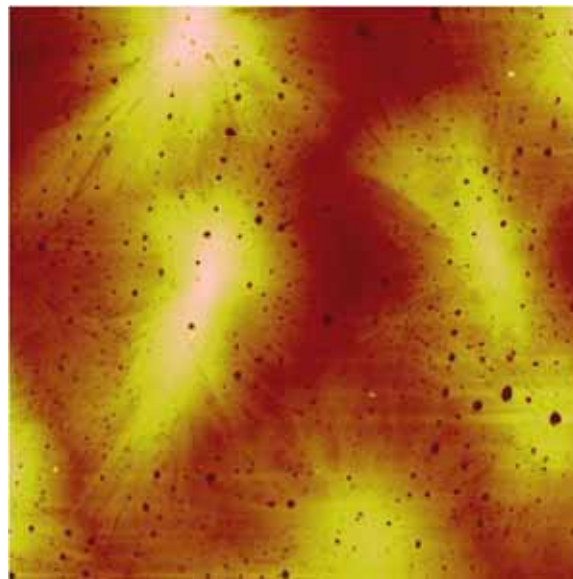


Figure 5. 11: AFM image of γ -phase spherulites with a scan size of $120 \times 120 \mu\text{m}^2$.

Figure 5.11 visualizes the bundle-like spherulites with different sizes. They are different from the spherulites formed by the α -phase and from the pure γ -phase, and are typical for the mixed structure of both α - and γ -phase. The same results were reported by Thomann et al. [12, 13] using polarized light microscopy and AFM in tapping mode after etching. These results indicate that AFM can be used to characterise propylene-ethylene random copolymers and obtain reliable results without etching.

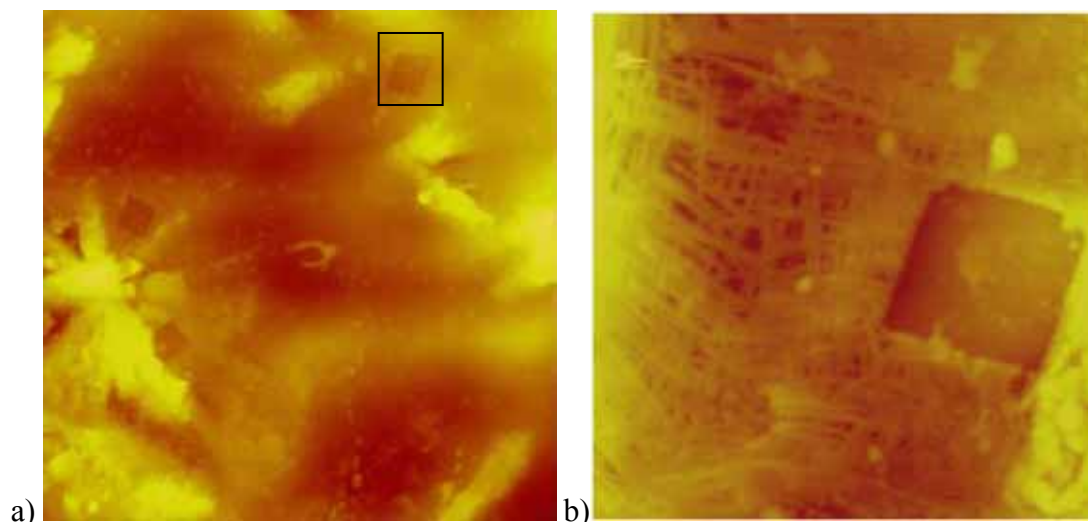


Figure 5. 12: a) AFM image of PPE1 with a scan size of $70 \times 70 \mu\text{m}^2$ and b) acquired from (a) as indicated with a box, scan size of $4.5 \times 4.5 \mu\text{m}^2$.

Figure 5.12a shows several γ -spherulites. Figure 5.12b shows the area between the γ -spherulites. It shows the cross-hatched lamellae of the α -modification tilted 80° to each other as result of the deposition of the helices of the same-handed ordinations along the b-axis of the unit cell of the α -phase.

Figure 5.12b also shows a lozenge-shaped structure, which is similar to that of polyethylene single crystals crystallized from solution [14]. Since this image was obtained on a sample contains 3.2% ethylene that was melt-crystallized at a slow cooling rate of $2^\circ\text{C}/\text{h}$ to room temperature, it can be assumed that this structure is a polyethylene single crystal. The slow cooling rate allows enough time for the polyethylene residues to accumulate to each other and form single crystals.

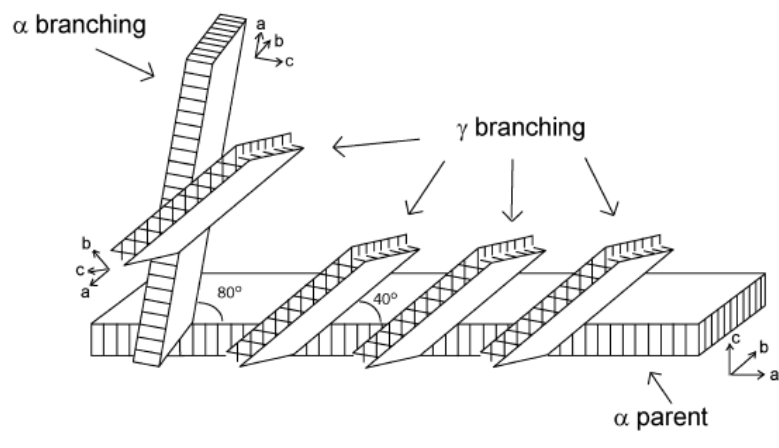
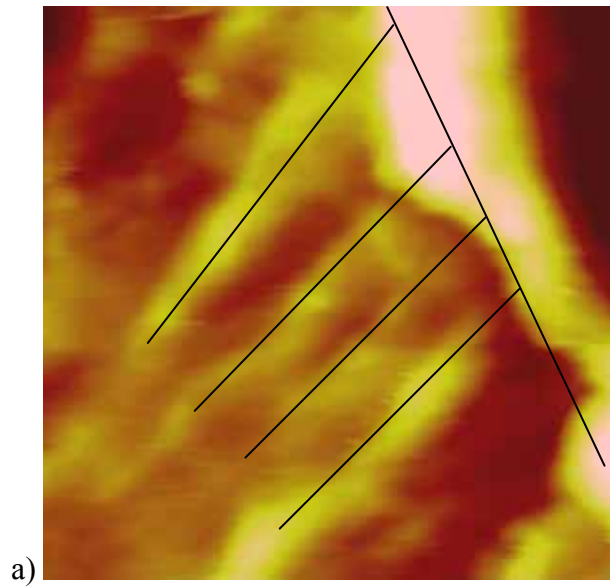


Figure 5.13: a) $1.3 \times 1.3 \mu\text{m}^2$ AFM image acquired in Figure 5.12, b) schematic model of α -iPP and γ -iPP branching from an α -‘parent’ lamella [2].

Figure 5.13a shows the epitaxial ongrowth of γ - lamellae on an α -lamella at an angle of approximately 45° . This observation is in a good agreement with the branching angle of 40° suggested by Stocker [8]. The α - γ branching occurs as a result of the deposition of a layer with the same-handed helices on the 010 face of the α -lamellae, followed by the typical structure of the γ -form, which consists of successive bilayers made of opposed-handed helices tilted 80° to each other.

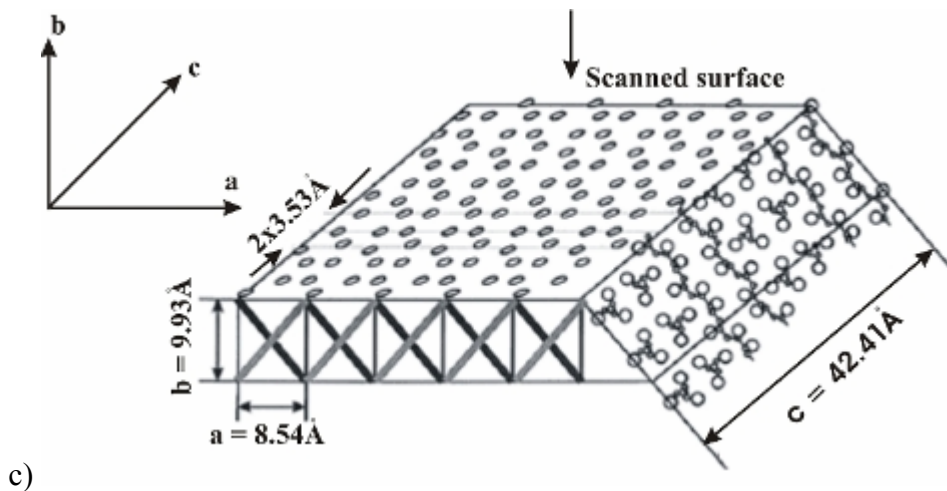
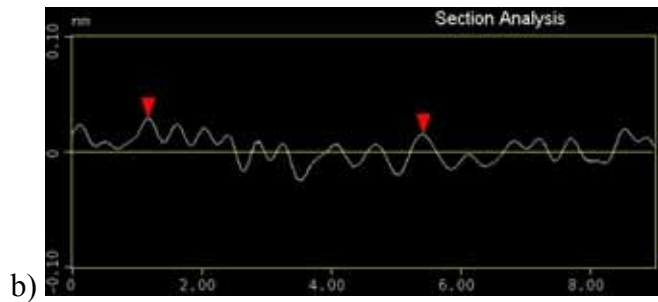
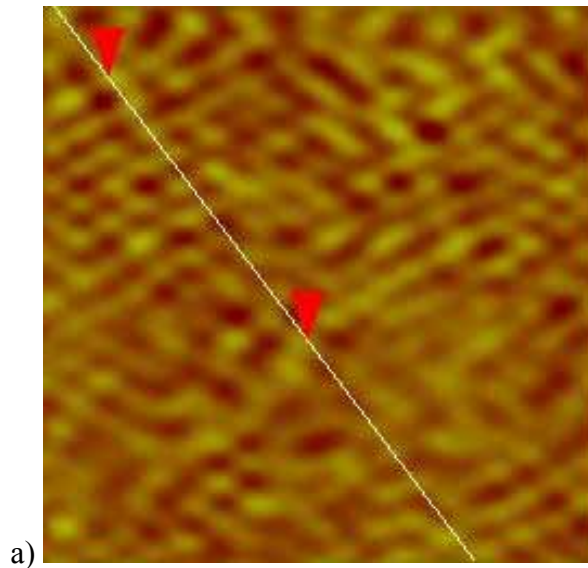


Figure 5. 14: a) High resolution image with a scan size of $7.1 \times 7.1 \text{ nm}^2$. The methyl groups are arranged in rows. b) the cross section along the line in a) showing the height profile of the methyl group, c) schematic drawing of the 110 plane of the γ -phase with dimensions and the arrangement of the helices [12].

Figure 5.14a shows the methyl groups as bright spots. Although they appear disordered, one can distinguish rows, which are oriented perpendicular to the direction of the indicated line. Figure 5.14b shows the height profile along the line drawn in a) across the rows of methyl groups. The average distance between 12 rows was about 42.52 Å, compared to 42.41 Å expected theoretically. The average spacing between the methyl groups is 3.8 Å in the (010) plane, which is close to the 3.53 Å reported by Brückner and Meille [3]. Figure 5.14c shows a schematic representation of the crystal lattice with dimensions and the arrangement of helices in the (110) plane of the γ -phase [12].

5.2.3 Propylene-ethylene block copolymers

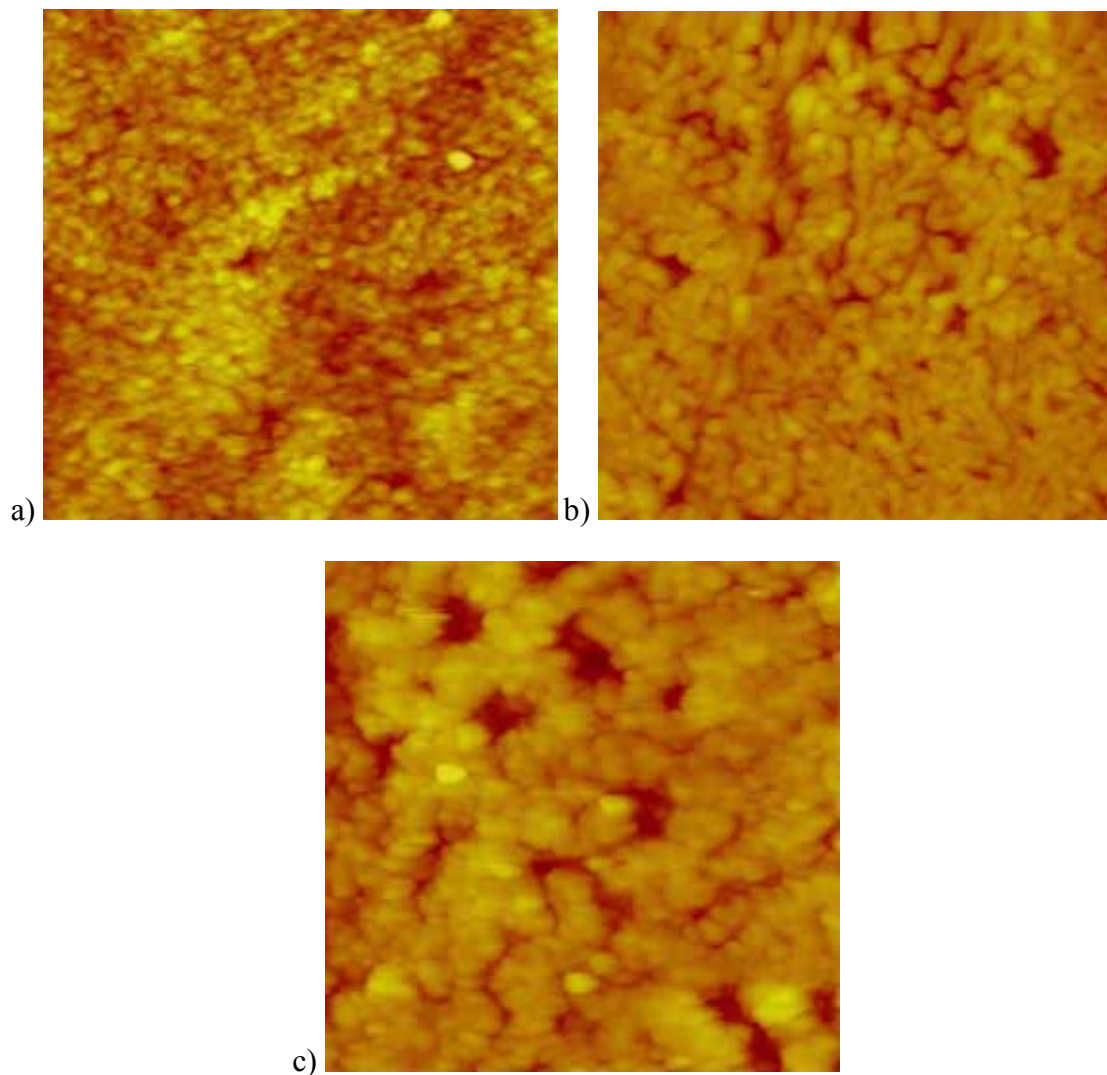


Figure 5. 15: AFM images of a) PEB1, b) PEB2 and c) PEB3 with a scan size $3 \times 3 \mu\text{m}^2$

The surface morphology of the propylene-ethylene block copolymers is presented in Figure 5.15. The images show a great variation in surface morphology, which could be related to the varying ethylene content since all the samples were prepared in the same way. The change in the morphology become more obvious as the ethylene content decreases from 12% to 6.5%, as can be seen in Figures 5.15a to 5.15c respectively.

Figure 5.15 shows several areas with regular structures, which could be the crystalline regions of polypropylene. The expected phase separation for this type of polypropylene copolymer was, however, not observed, which disagrees with results obtained from SEM after etching the amorphous layers away by Hongsheng et al. [15]. Figure 5.15a shows small lath-like crystal structures, which can be compared to the larger lath-like structures in Figure 5.15b. The size of these structures seems to depend on the ethylene concentration.

Figure 5.16 shows the high resolution AFM images of the propylene-ethylene block copolymer sample PEB3. Both the four and the five pattern of the a-c (010) plane of the α -phase were observed in this same sample.

Figure 5.16a represents the regular structure of the five pattern of the a-c (010) plane of the α -phase with the angle $\beta \approx 79.2^\circ$. The average dimensions of the unit cell are $a = 6.08 \text{ \AA}$ and $c = 6.02 \text{ \AA}$ with errors of 8.57 % and 7.32% respectively.

5.16b shows the regular structure of the four pattern of the same plane which can be related to α -phase, but the parameters of the unit cell are slightly larger than expected from the literature [3, 4]. The angle β is about 82.1° and the average dimensions of the unit cell are $a = 7.11 \text{ \AA}$ and $c = 7.05 \text{ \AA}$ with errors of 6.91% and 8.46% respectively. These results were confirmed by X-ray results, in which the α -phase represented 100% of the crystalline regions. A model produced with X-seed to illustrate the a-c plane of the α -phase crystal structure with the four pattern is displayed in Figure 5.16c.

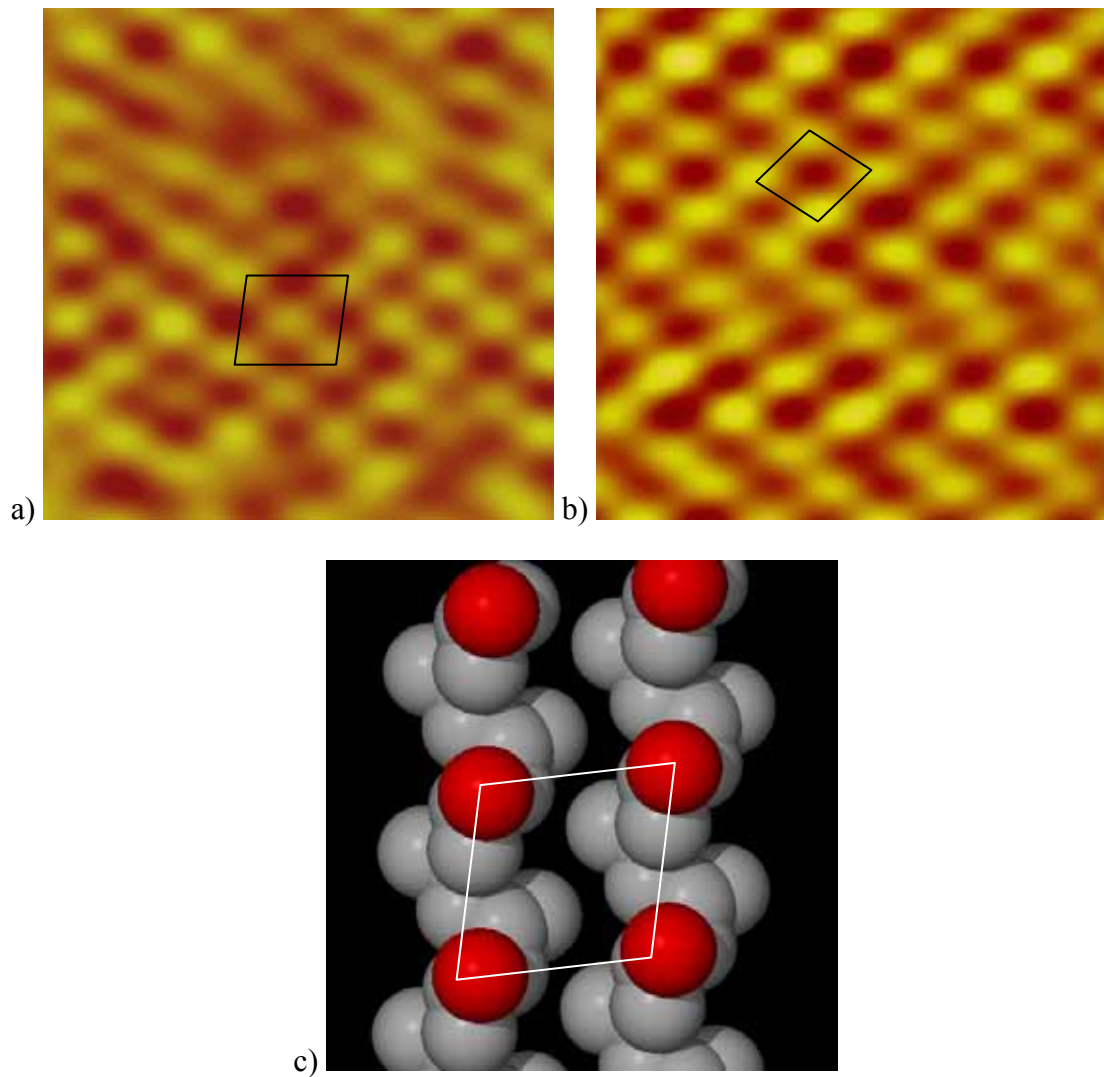


Figure 5.16: high resolution AFM image of PEB1 a) $6 \times 6 \text{ nm}^2$, b) $3 \times 3 \text{ nm}^2$ and c) model produced with X-seed to illustrate the ac plane of a α -phase crystal (Four pattern) [7].

5.2.4 Propylene-pentene random copolymers

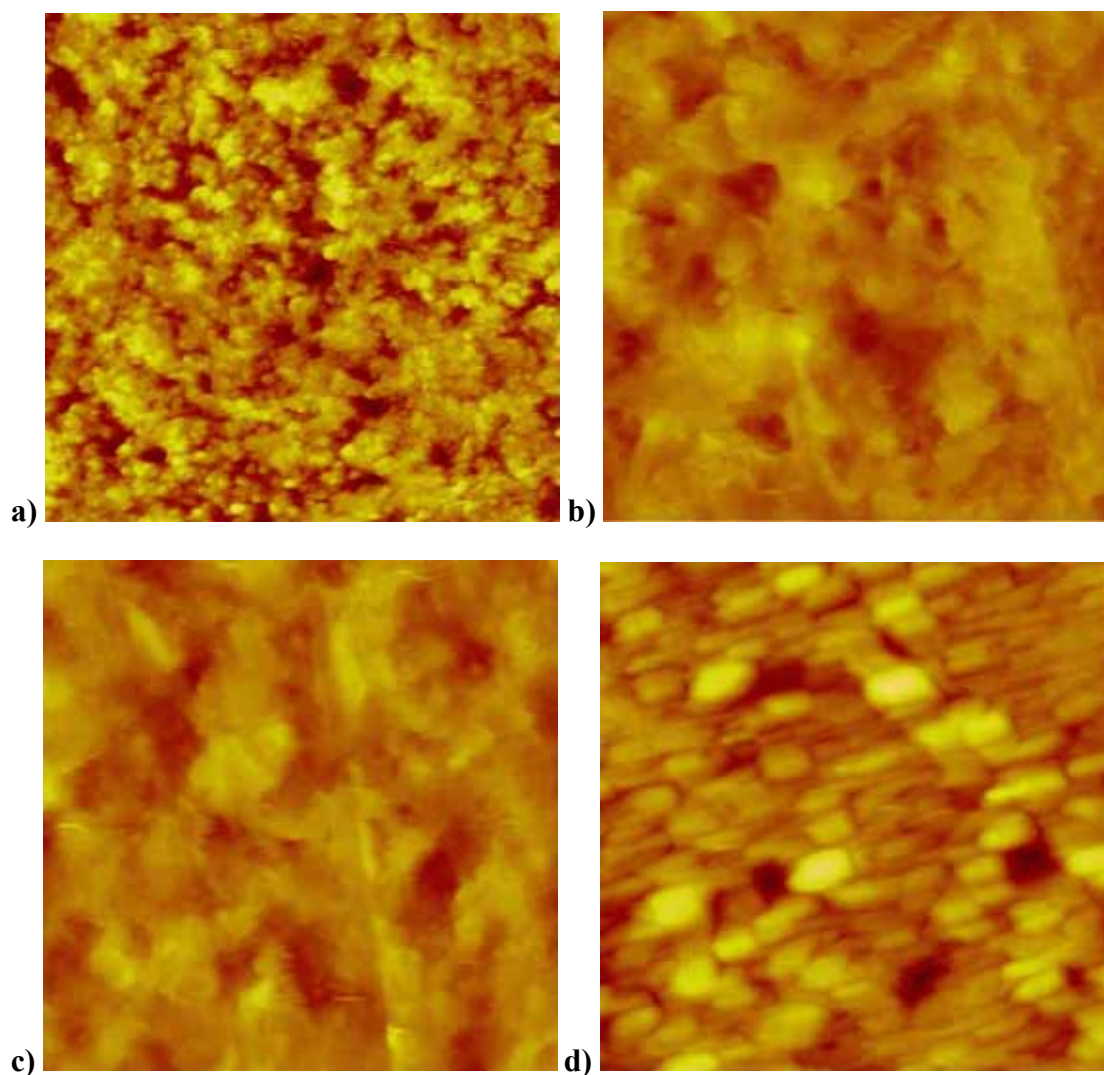


Figure 5. 17: 12.5x12.5 μm^2 AFM images of a) PPe1, PPe2, PPe3 and PPe4.

The propylene-pentene random copolymer samples contained different amounts of pentene, which resulted in different γ -phase contents as displayed in Figure 5.17. The surface of the sample PPe1, which contains 2.29 mol % pentene and 52.18% of the γ -phase, is shown in Figure 5.17a. It presents a sponge-like morphology with a lamellar size smaller than that sample of PPe4. Samples PPe2 and PPe3 with 1.18 mol % and 1.75mole % pentene and 41.28% and 47.06% γ -phase content respectively show a similar morphology (Figure 5.17b and 5.17c). Figure 5.17d shows the morphology of PPe4 with 22.86 mol % pentene and 0.92% γ -phase content. It shows a lath-like lamellar structure with varying thickness.

Figure 5.17 also shows different crystal structures, which are influenced by the

presence of the comonomer (1-pentene) and other defects. The maximum crystallisable sequence length and the ability to propagate long radial oriented lamellae of α - or γ -crystals is restricted by these defects. Depending on the concentration of the comonomer the spherulitic lamellar arrangements are disrupted [2]. This explains the difference between the Figures 5.17a and 5.17d where the comonomer concentration decreases, which leads to less disruption lamellar arrangements.

Unfortunately no clear high resolution images could be obtained on these samples. This was due to difficulties, such as slipping of the AFM tip the surface and repulsion of the tip, which was caused by irregularities of the sample surface.

5.3 Attempted quantification of the crystallinity degree

The crystallinity degree of the various samples was calculated from high resolution images and compared to the X-ray results.

The degree of crystallinity was determined as a percentage of the image area that contained regular structures. In order to do this, each image of $6 \times 6 \text{ nm}^2$ was divided into nine squares of $2 \times 2 \text{ nm}^2$, as shown in Figure 5.18.

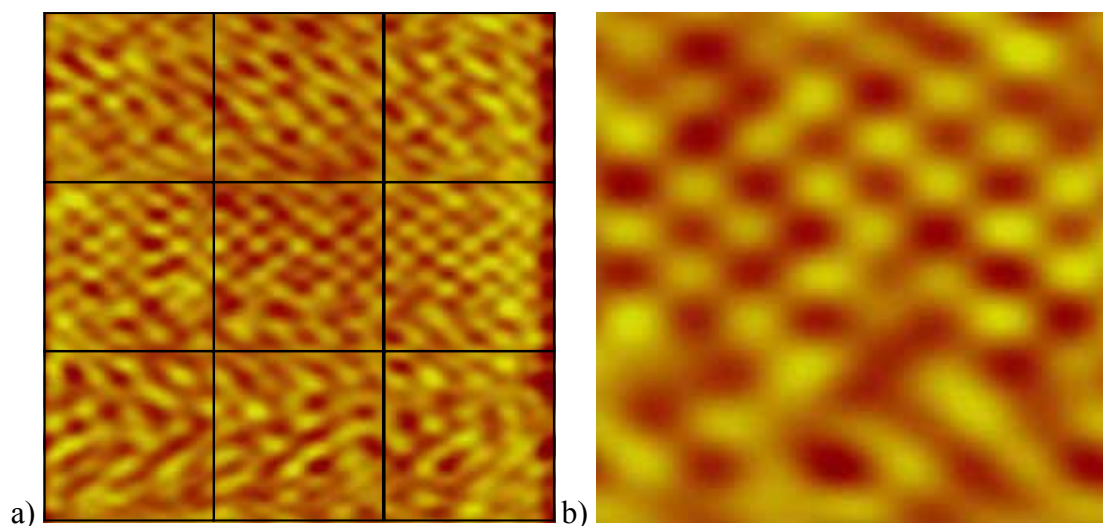


Figure 5.18: a) High resolution AFM image with a scan range of $6 \times 6 \text{ nm}^2$, b) magnified image with a scan range of $2 \times 2 \text{ nm}^2$.

The surface area of these squares represents the total area containing amorphous and crystalline regions. The area within each square with regular structures represents the crystalline area. The degree of crystallinity was calculated according to equation 5.1:

$$\text{Degree of crystallinity} = \text{crystalline area} / \text{total area of the image} \quad \text{Eq. 5.1}$$

This equation was applied to each one of the nine squares and the average was then calculated. This was done for all the high resolution images that showed any regular structures, whether it was α - or γ -phase. The resulting crystallinity degrees are presented in Table 5.5-5.9.

Table 5. 5: Estimation of the average degree of crystallinity for iPP.

Total area / nm²	Crystalline Area / nm²	Degree of crystallinity %
4.00	1.81	45.25
4.00	1.37	34.25
4.00	1.17	29.25
4.00	3.24	81.00
4.00	2.70	67.50
4.00	3.00	75.00
4.00	2.39	59.75
4.00	1.37	34.25
4.00	1.78	44.50
Average		52.30

Table 5.5 shows the total area of each square, the crystalline area and the calculated degree of crystallinity for the iPP sample.

The average calculated degree of crystallinity is 52.30% \pm 18. The X-ray results for the same sample gave a value of 57.20%, which agrees well with the degree of crystallinity determined by AFM. The large deviations from the average value could be explained by the fact the AFM results were obtained only on the surface layer of the sample. Due to segregation processes the amount of the amorphous phase on the surface could be higher than in the bulk of the sample. This leads to a more heterogeneous surface in contrast to the fairly uniform crystal structure in the bulk. Additionally environmental contaminates and the interface to a different medium could influence the degree of the crystallinity on the surface.

Table 5. 6: Estimation of the average degree of crystallinity for PPE5.

Total area / nm²	Crystalline Area / nm²	Degree of crystallinity %
4.00	1.79	44.75
4.00	1.23	30.75
4.00	1.11	27.75
4.00	2.75	68.75
4.00	2.81	70.25
4.00	2.91	72.75
4.00	2.24	56.00
4.00	1.32	33.00
4.00	1.61	40.25
Average		49.36

Table 5.6 shows the calculated degree of crystallinity for the sample PPE5. It is 49.36% \pm 17. The X-ray results for the same sample gave a value of 63.30% crystallinity, which differs considerably from the AFM result. The much lower degree of crystallinity obtained by AFM could again be explained by surface effects.

Table 5. 7: Estimation of the average degree of crystallinity for PPE1.

Total area / nm²	Crystalline Area / nm²	Degree of crystallinity %
4.00	1.07	26.75
4.00	2.25	56.25
4.00	1.65	41.25
4.00	2.67	66.75
4.00	3.84	96.00
4.00	2.57	64.25
4.00	2.61	65.25
4.00	2.90	72.50
4.00	1.40	35.00
Average		55.22

Table 5.7 presents the total area, the crystalline area and the degree of crystallinity of a propylene-ethylene random copolymer, with the sample code sample PPE1. As can be seen, the average degree of crystallinity determined with AFM is approximately 55.22% \pm 20, which compares well to the 52.78% obtained from X-ray measurements. Although the estimated degree of crystallinity is close to the actual value, it is larger than the value obtained from X-ray, which can be explained by the fact that only crystalline areas of the surface were imaged by AFM.

For the polypropylene-ethylene block copolymer PEB3 the degree of crystallinity was

calculated based on two images, where each image represents one possible face (four or five pattern) of the 010 plane of the α -phase.

Table 5. 8: Estimation of the average degree of crystallinity for PEB3 of the surface showing the four pattern (a).

Total area / nm²	Crystalline area / nm²	Degree of crystallinity %
4.00	1.66	41.50
4.00	2.13	53.25
4.00	2.13	53.25
4.00	2.30	57.50
4.00	2.77	69.25
4.00	2.88	72.00
4.00	2.28	57.00
4.00	2.65	66.25
4.00	2.15	53.75
Average		58.19

Table 5. 9: Estimation of the average degree of crystallinity for PBE3 of the surface showing of five pattern (b).

Total area / nm²	Crystalline area / nm²	Degree of crystallinity %
4.00	2.19	54.75
4.00	2.07	51.75
4.00	2.12	53.00
4.00	2.98	74.50
4.00	2.50	62.50
4.00	2.48	62.00
4.00	2.74	68.50
4.00	2.54	63.50
4.00	2.00	50.00
Average		60.05

Table 5.8 and 5.9 present the total area, the crystalline area and the degree of crystallinity for the sample PEB3, with the two different surface modifications showing a four and five pattern respectively. Two different values for the degree of crystallinity were obtained, where the degree of crystallinity for the four patterned surface (a) was lower than for the five patterned surface (b). The obtained values were $58.19\% \pm 8.9$ and $60.05\% \pm 7.8$ respectively. Both of these values are lower than the degree of crystallinity determined by X-ray, which was 65 %. They are, however, in a comparable range and the deviation can be explained by surface effects.

Generally the degree of crystallinity obtained by AFM was lower than the value obtained from WAXD analysis. This can be explained by the fact that AFM takes only the surface layer into account where the crystalline order is disturbed by the interface between polymer and air and where the degree of crystallinity might be lower due to segregation of amorphous chain segments.

5.4 References

1. R. G. Alamo, M. H. Kim, M. J. Galante, J. R. Isasi, L. Mandelkern. *Structural and kinetic factors governing the formation of the γ -polymorph of isotactic polypropylene*. *Macromolecules*. 1999, **32**, 4050-4064.
2. I. L. Hosier, R. G. Alamo, J. S. Lin. *Lamellar morphology of random metallocene propylene copolymers studied by atomic force microscopy*. *Polymer*. 2004, **45**, 3441–3455.
3. S. Brückner, S. V. Meille, V. Petraccone, B. Pirozzi. *Polymorphism of isotactic polypropylene*. *Progress in Polymer Science*. 1991, **16**, 361-404.
4. B. Lotz, C. Wittmann, A. J. Lovinger. *Structure and morphology of poly(propylenes): a molecular analysis*. *Polymer*. 1996, **22**, 4979-4992.
5. F. J. Padden, J. D. Keith. *Spherulitic crystallization in polypropylene*. *Journal of Applied Physics*. 1959, **30**, 1479-1484.
6. D. R. Norton, A. Keller. *The spherulitic and lamellar morphology of melt-crystallized isotactic polypropylene*. *Polymer*. 1985, **26**, 704-716.
7. L. J. Barbour. *X-Seed - A software tool for supramolecular crystallography*. *Journal of Supramolecular Chemistry*. 2001, **1**, 189-191.
8. W. Stocker, S. N. Magonov, H. J. Cantow, J. C. Wittmann, B. Lotz. *Contact faces of epitaxially crystallized α - and γ -phase isotactic polypropylene observed by atomic force microscopy*. *Macromolecules*. 1993, **26**, 5915-5923.
9. I. Masada, T. Okihara, S. Murakami, M. Ohara, A. Kawaguchi, K. Katayama. *A bimodal structure of solution-grown isotactic polypropylene with orthanonally crossed lamellae*. *Journal of Polymer Science Part B: Polymer Physics*. 1993, **31**, 843-852.
10. B. Lotz, J. C. Wittmann. *The molecular origin of lamellar branching in the α (monoclinic) form of isotactic polypropylene*. *Journal of Polymer Science Part B: Polymer Physics*. 1986, **24**, 1541-1558.
11. K. Mezghani, P. J. Phillips. *The γ -phase of high molecularweight isotactic polypropylene. II: The morphology of the γ -form crystallized at 200MPa*. *Polymer*. 1997, **38**, 5725-5733.
12. R. Thomann, C. Wang, J. Kressler, R. Muelhaupt. *On the γ -phase of isotactic polypropylene*. *Macromolecules*. 1996, **29**, 8425-8434.
13. R. Thomann, H. Semke, R. D. Maier, Y. Thomann, J. Scherble, R. Muelhaupt,

- J. Kressler. *Influence of stereoirregularities on the formation of the γ -phase in isotactic polypropene*. *Polymer*. 2001, **42** 4597-4603.
14. S. N. Magonov, N. A. Yerina, G. Unger, D. H. Reneker, D. A. Lvanov. *Chain unfolding in single crystals of ultralong alkane $C_{390}H_{782}$ and polyethylene: An Atomic force microscopy study*. *Macromolecules*. 2003, **36**, 5637-5649.
15. H. Tan, L. Li, Z. Chen, Y. Song, Q. Zheng. *Phase morphology and impact toughness of impact polypropylene copolymer*. *Polymer*. 2005, **46**, 3522-3527.

6 Conclusions and Scope of Future Work

6.1 Conclusions

The results show that the surface morphology of the investigated polymers can be observed with AFM at a molecular level without any special sample preparation of the polymeric films. Both the α - and γ -phase of iPP have been successfully imaged and identified without prior treatment of the surface.

The mass crystallinity of the α - and γ -phase content was determined by WAXD for isotactic polypropylene, propylene-ethylene random copolymers, propylene-ethylene block copolymers and propylene-pentene random copolymers.

These results were compared to AFM results, where the degree of crystallinity was calculated as a percentage of the surface area exhibiting regular structures. The results obtained by the two techniques compare well, although the values obtained by AFM tended to be lower than the values determined by WAXD.

Images of the propylene-ethylene random copolymers showed that the γ -phase content increased with the ethylene content. On the other hand it seems that the ethylene content in the propylene-ethylene block copolymers had no effect on the γ -phase content. In the case of propylene-pentene random copolymers, the γ -phase content increased as the pentene content increased.

In general AFM proved to be a valuable tool to image polypropylene surfaces and to determine the degree of crystallinity and the crystal configuration.

Spherulites with diameters ranging from 10-30 μ m were imaged on propylene-ethylene random copolymer surfaces. In these spherulites the lamellae could be observed in radial direction with an average thickness of 65nm.

The cross-hatching phenomenon of isotactic polypropylene was observed for samples containing both α - and γ -phase, where the α - α branching angle of 80 $^\circ$ could easily be distinguished from the α - γ branching angle of 40 $^\circ$.

Two types of γ -phase spherulites were observed, namely a feather-like form for

samples with a high content of the γ -phase and a bundle-like form with varying sizes, which is typical for the mixed structure of both α - and γ -forms.

The α - and γ -phase were investigated by obtaining high resolution images. Although it was difficult to obtain clear images due to noise, it was possible to distinguish between the α - and γ -phase.

For the α -phase in propylene-ethylene random copolymers, for example, the dimensions agreed well to the values given in literature [1-3]. The angles of the lozenge were found to be 101° and 79° and the dimensions of the unit cell were $a = 5.98 \text{ \AA}$ and $c = 6.12 \text{ \AA}$.

Similarly the dimensions of the γ -phase compared well to results from Thomann et al. [4], where the average distance between 12 of the methyl group rows was about 42.41 \AA , compared to 42.52 \AA determined in this study. The average spacing between the methyl groups was 3.8 \AA in the (010) plane, which is close to the 3.53 \AA reported by Brückner and Meille [5].

In some images of PPE1 a lozenge-shaped structure could be observed between several γ -spherulites, which is similar to that of polyethylene single crystal crystallized from solution. Since this sample contains 3.2% ethylene, this could be explained as a result of the slow cooling rate, which led to the formation of single crystals of polyethylene.

In summary this work has met its main objectives to identify both the α - and the γ -phase of different polypropylene samples without any further preparation or treatment of the surface after melt crystallisation.

It was also possible to quantify the amount of crystalline area, although the values obtained from the surface by AFM were generally lower than the bulk values obtained by WAXD.

6.2 Suggested future work

1) The degree of crystallinity was estimated from only a few high resolution images, which might explain the differences with regard to X-ray results. Further work should be carried out to confirm these results, using a larger number of AFM images in order

to obtain statistical satisfactory results.

2) Further investigation should be carried out in order to identify and explain the appearance of the lozenge-shaped structures between the γ -spherulites in polypropylene-ethylene copolymers, which might result from the slow cooling rate of the sample that led to the formation of single crystals of polyethylene.

3) Other semi-crystalline polymers, such as polyethylene, polybutene-1 or polyester could be investigated by the methods used in this work.

6.3 References

1. B. Lotz, C. Wittmann, A. J. Lovinger. *Structure and morphology of poly(propylenes): a molecular analysis*. Polymer. 1996, **22**, 4979-4992.
2. S. Brückner, S. V. Meille, V. Petraccone, B. Pirozzi. *Polymorphism of isotactic polypropylene*. Progress in Polymer Science. 1991, **16**, 361-404.
3. W. Stocker, S. N. Magonov, H. J. Cantow, J. C. Wittmann, B. Lotz. *Contact faces of epitaxially crystallized α - and γ -Phase isotactic polypropylene observed by atomic force microscopy*. Macromolecules. 1993, **26**, 5915-5923.
4. R. Thomann, C. Wang, J. Kressler, R. Muelhaupt. *On the γ -phase of isotactic polypropylene*. Macromolecules. 1996, **29**, 8425-8434.
5. S. V. Meille, S. Brückner, W. Porzio. *γ -Isotactic Polypropylene. A Structure with nonparallel chain axes*. Macromolecules. 1990, **23**, 4114-4121.